Table of Contents

Materials

4-(Diphenylphosphino)styrene (97 %, Sigma Aldrich), dichloro(1,5-cyclooctadiene) platinum(II) (99 %, Alfa Aesar), aniline (99+ %, Alfa Aesar), ferrocene (98 %, Sigma Aldrich), bis(diphenylphosphino)methane (97 %, abcr) and allyl alcohol (99 %, Sigma Aldrich) were used as received. Styrene (99 %, Merck) was passed through a column of basic alumina (Acros) and stored at -19 °C. Deuterated solvents ($CDCl_3$ and C_6D_6) were obtained from Carl Roth GmbH (99.5 atom % D). $CDCl_3$ was distilled, degassed and stored over molecular sieves (4 Å). Dimethyl formamide (DMF), methanol (MeOH), dichloromethane (DCM) and tetrahydrofuran (THF) were purchased as analytical grade and used as received.

4-(Diphenylphosphine oxide)styrene,[1] $[Eu(dbm)_3(H_2O)_2]$,[2] $[Eu(tta)_3(H_2O)_2]$[3] and 2,2,6,6-tetramethyl-1-(1-phenylethoxy)piperidine[4] were synthesized according to literature procedures.

Instrumentation

NMR spectra were recorded on a Bruker Avance 400 (400 MHz) spectrometer. Chemical shifts δ [ppm] were referenced to the residual solvent resonances and are reported relative to external tetramethylsilane (^1H), $CFCl_3$ (^{19}F), 85 % H_3PO_4 (^{31}P) or 1.2 M Na_2PtCl_6 in D_2O (^{195}Pt). Abbreviations used in the compounds' analysis include singlet (s), broad singlet (bs), doublet (d), triplet (t) and multiplet (m). The diffusion coefficients were measured using a Bruker 400 MHz Avance III HD spectrometer on a BBIF inversely detected $^1H/^{19}F$, BB double resonance room temperature probe head with actively shielded z-gradients. The temperature was controlled via a Bruker Smart VT unit and was calibrated to be exactly 298 K. The diffusion coefficients were measured with Diffusion Ordered NMR Spectroscopy (DOSY) experiments using bipolar gradient pulses and stimulated echo with or without longitudinal eddy current delay (STEBP or LEDBP).

Size-exclusion chromatography (SEC) measurements were performed on a PL-SEC 50 Plus (Polymer Laboratories, Varian), running on tetrahydrofuran (THF) (HPLC-grade). The applied columns were a PLgel Mixed C guard column (50 × 7.5 mm), followed by three PLgel Mixed C linear columns (300 × 7.5 mm, 5 μm beadsize) and a differential refractive index (RI) detector. The device was operated at 35 °C column temperature with a flow rate of 1 $mL \cdot min^{-1}$. The columns were calibrated using linear polystyrene standards ranging from 476 to 2.5×10^6 $g \cdot mol^{-1}$. The measured samples were dissolved in THF (2 $mg \cdot mL^{-1}$) and filtered through PTFE membranes with a pore size of 0.2 μm prior to injection. To obtain M_n and $Đ$ values, the integration of the polymer peak was carried out from low elution times to approximately 40 minutes due to overlap with an SEC system peak. No baseline correction was performed. Consequently, M_n and $Đ$ values are estimates.

IR spectra were obtained on a Bruker Tensor 37 FTIR spectrometer, equipped with a room temperature DLaTGS detector and a diamond ATR (attenuated total reflection) unit. Abbreviations used in the compounds' analysis include very strong (vs), strong (s), medium (m), weak (w) and very weak (vw).

Photoluminescence (PL) measurements were performed with a PTI QuantaMaster™ 8000 series spectrometer, equipped with multiple illuminators and double emission monochromator with R928 PTM, InGaAs and InSb detector and a continuous 75 W xenon lamp. At 295 K the solid samples (crystalline powders) were measured as dispersions in a thin layer of viscous mineral oil (Sigma Aldrich), placed between 1 mm quartz plates (Material: Spectrosil®2000).

Abbreviations

approx.	approximately
ATR	attenuated total reflection
COD	cyclooctadiene
Đ	dispersity
dbm	dibenzoylmethanide
DCM	dichloromethane
DMF	dimethyl formamide
DOSY	Diffusion Ordered Spectroscopy
DPPM	bis(diphenylphosphino)methane
equiv.	equivalents
IR	infra-red
MeOH	methanol
NMP	Nitroxide-mediated radical polymerization
NMR	nuclear magnetic resonance
PL	photoluminescence
RI	refractive index
SCNP	single-chain nanoparticle
SEC	size exclusion chromatography
THF	tetrahydrofuran
tta	thenoyltrifluoroacetonate
UV-Vis	ultraviolet-visible

Synthesis

Synthesis of Terpolymer $P_{P/Oxide}$

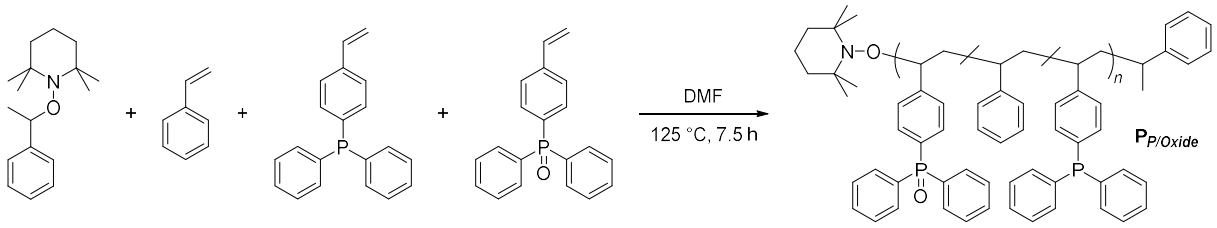

Scheme S1. Nitroxide mediated polymerization of styrene, 4-(diphenylphosphino)styrene and 4-(diphenylphosphine oxide)styrene, applying the initiator 2,2,6,6-tetramethyl-1-(1-phenylethoxy)piperidine, resulting in terpolymer poly(styrene-co-4-(diphenylphosphino)styrene-co-4-(diphenylphosphine oxide)styrene (**$P_{P/Oxide}$**).

A photovial was equipped with styrene (4.36 g, 41.9 mmol, 735 equiv.), 4-(diphenylphosphino)styrene (460 mg, 1.60 mmol, 28.0 equiv.), 4-(diphenylphosphine oxide)styrene[1] (121 mg, 0.40 mmol, 7.00 equiv.) and 2,2,6,6-tetramethyl-1-(1-phenylethoxy)piperidine[4] (15.0 mg, 0.06 mmol, 1.00 equiv.). After dissolving the compounds in 1.45 mL dry DMF, the vial was purged with argon for 1 hour. Stirring the reaction mixture, the vial was heated at 125 °C for 7.5 hours. Afterwards, the reaction was quenched by cooling to ambient temperature and opening the vial to air. Repeated precipitation (three times) into cold MeOH yielded the final polymer as a white powder. Yield: 2.10 g.

Characterization via ^{1}H and ^{31}P{^{1}H} NMR analyses revealed a monomer ratio between styrene, 4-(diphenylphosphino)styrene and 4-(diphenylphosphine oxide)styrene of approx. 57:2:1. Thus, 1.7 % of phosphine oxide and 3.5 % of phosphine side groups were statistically implemented into the polymer chain (results in 0.16 mmol phosphine oxide species and 0.32 mmol phosphine species per 1 g of terpolymer **$P_{P/Oxide}$**). The given values are – within the margin of error of NMR spectroscopy – estimates which are additionally hampered by the solvent resonance ($CHCl_3$) in the ^{1}H NMR spectrum. Additional NMR experiments, as to the issue of an accurate distinction between triarylphosphine and triarylphosphine oxide moieties, were performed (see Fig. S17 to S20).

^{31}P{^{1}H} NMR experiments, applying bis(diphenylphosphino)methane (DPPM) as an external standard, resulted in 0.17 mmol phosphine oxide species and 0.35 mmol phosphine species per 1 g of terpolymer **$P_{P/Oxide}$** (refer to Fig. S21), thus confirming the priorly obtained values.

SEC characterization (THF, RI): M_n = 25 300 g·mol^{-1}, $Đ$ = 1.41.

^{1}H NMR (400 MHz, $CDCl_3$): δ [ppm] = 7.70–7.19 (m, aromatic protons of 4-(diphenylphosphino)styrene and 4-(diphenylphosphine oxide)styrene), 7.19–6.20 (m, aromatic protons of styrene), 2.40–0.99 (m, aliphatic protons, backbone).

^{31}P{^{1}H} NMR (162 MHz, $CDCl_3$): δ [ppm] = 29.2 (s, O=*P*Ph$_2$Ar), -6.24 (s, *P*Ph$_2$Ar).

IR (ATR): $\tilde{\nu}$ [cm^{-1}] = 3082 (w), 3059 (w), 3025 (m), 3001 (vw), 2922 (m), 2848 (w), 1601 (m), 1584 (vw), 1493 (s), 1452 (s), 1437 (m), 1373 (vw), 1202 (w), 1182 (vw), 1155 (vw), 1118 (w), 1069 (vw), 1028 (w), 907 (vw), 842 (vw), 826 (vw), 756 (s), 748 (s), 697 (vs), 541 (m), 506 (vw).

Synthesis of Heterometallic Eu(III)/Pt(II)-SCNPs

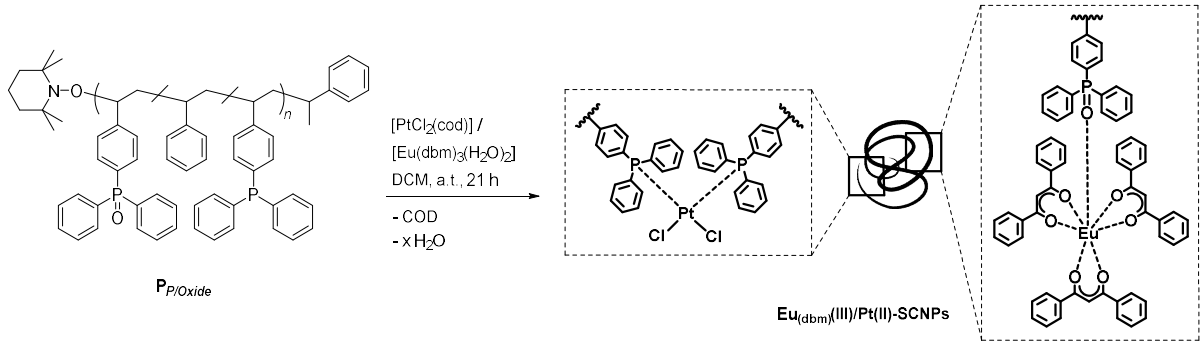

Scheme S2. Formation of heterometallic SCNPs applying the bifunctional terpolymer $\mathbf{P_{P/Oxide}}$ and the metal precursors $[PtCl_2(cod)]$ and $[Eu(dbm)_3(H_2O)_2]$ in a one-pot reaction. The metal species coordinate orthogonally to the respective ligands of the polymer scaffold, yielding fluorescent and catalytic active **$Eu_{(dbm)}$(III)/Pt(II)-SCNPs**. Whereas the Eu(III) species is most likely coordinated in a 1:1 metal-to-ligand ratio, the coordination of the platinum(II) ions proceeds in a 2:1 ligand-metal ratio, resulting in a single-chain collapse.

$\mathbf{P_{P/Oxide}}$ (50.0 mg, 7.90 µmol phosphine oxide functional groups, 15.8 µmol phosphine functional groups, 1.00 equiv.) was dissolved in 20.0 mL dry DCM and purged with argon for 5 min. In a separate 250 mL flask, the precursor complexes $[Eu(dbm)_3(H_2O)_2]$[2] (6.77 mg, 7.90 µmol, 1.00 equiv. with regards to the phosphine oxide moieties) and $[PtCl_2(cod)]$ (2.95 mg, 7.90 µmol, 0.50 equiv. with regards to the phosphine moieties) were dissolved in 150 mL dry DCM and purged with argon for 30 min. Applying a syringe pump, the polymer solution was added to the solution of metal ions over a time period of 20 hours (dropping rate ~ 1 mL·hour^{-1}). After complete addition, the solution was stirred for another hour, and subsequently concentrated under reduced pressure (to 1-2 mL). The remaining solution was precipitated into cold MeOH and stirred for 1 hour. After filtration **$Eu_{(dbm)}$(III)/Pt(II)-SCNPs** were received as a white powder.

SEC characterization (THF, RI): M_n = 20 200 g·mol^{-1}, $Đ$ = 1.49. – The linkages between Eu(III) and the phosphine oxide units in the polymer chain are, to some extent, not strong enough to withstand the harsh conditions of SEC measurement, as an additional signal at high retention times is observed, which is attributed to the molecular Eu(III) complex. Therefore, the above stated results rather represent Pt(II)-linked SCNPs exhibiting non-coordinated phosphine oxide moieties.

^{1}H NMR (400 MHz, $CDCl_3$): δ [ppm] = 16.89 (s, Eu(dbm)$_3$-C*H*), 8.08–7.97 (m, Eu(dbm)$_3$-Ph), 7.78–6.07 (m, aromatic protons of all incorporated monomers), 7.61–7.47 (m, Eu(dbm)$_3$-Ph), 2.45–0.65 (m, aliphatic protons, backbone).

^{31}P{^{1}H} NMR (162 MHz, $CDCl_3$): δ [ppm] = 29.1 (s, Eu-O=*P*Ph$_2$Ar), 19.5 (*trans*-(*P*Ph$_2$Ar)$_2$-PtCl$_2$), 13.5 (d, $^1J_{P,Pt}$ = 3661 Hz, *cis*-(*P*Ph$_2$Ar)$_2$-PtCl$_2$). – *cis*/*trans*-ratio approx. 30:1. Due to the low amount, no ^{195}Pt satellites are detected for the *trans*-species.

^{195}Pt NMR (86 MHz, $CDCl_3$): δ [ppm] = -4420 (t, $^1J_{Pt,P}$ = 3715 Hz, *cis*). – Due to the low amount of *trans*-species, no corresponding resonance is detected.

IR (ATR): $\tilde{\nu}$ [cm^{-1}] = 3082 (vw), 3059 (w), 3025 (m), 3001 (vw), 2923 (s), 2849 (w), 1600 (m), 1549 (vw), 1519 (vw), 1493 (s), 1452 (s), 1438 (m), 1405 (vw), 1377 (vw), 1312 (vw), 1262 (vw), 1202 (vw), 1183 (vw), 1155 (vw), 1119 (vw), 1097 (w), 1069 (vw), 1028 (w), 1002 (vw), 907 (vw), 753 (m), 697 (vs), 542 (m), 522 (w).

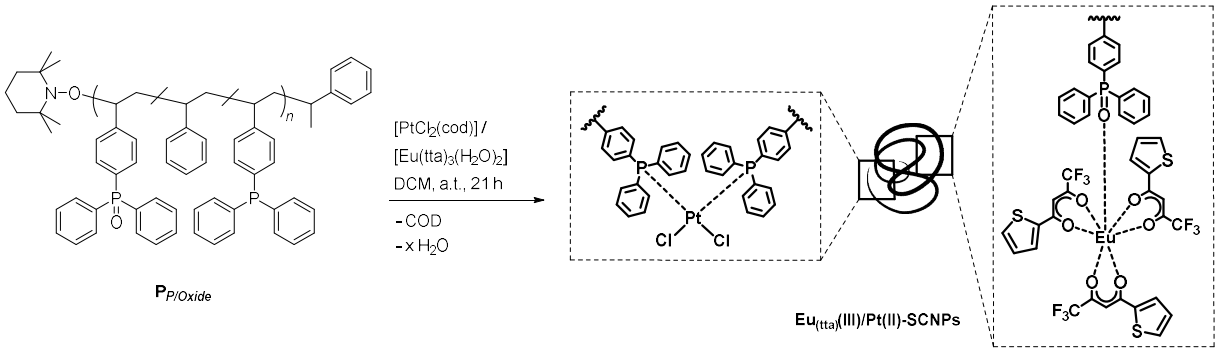

Scheme S3. Synthesis of **Eu$_{(tta)}$(III)/Pt(II)-SCNPs** via the same reaction pathway as described in Scheme S2.

Following the same reaction procedure as described in Scheme S2, different heterometallic **Eu$_{(tta)}$(III)/Pt(II)-SCNPs** were synthesized, applying the Eu(III) precursor [Eu(tta)$_3$(H$_2$O)] (tta = thenoyltrifluoroacetonate). The non-symmetric tta moiety of the Eu(III) species results in a visibly more intense luminescent behavior of the corresponding nanoparticles.

^{1}H NMR (400 MHz, CDCl$_3$): δ [ppm] = 8.02–5.87 (m, aromatic protons of all incorporated monomers), 2.52–0.61 (m, aliphatic protons, backbone). – Due to the paramagnetic properties of the Eu(III) species the proton resonances for the thenoyltrifluoroacetonate (tta) ligands cannot be resolved and overlay partially with the aromatic proton resonances of the terpolymer.

^{31}P{^{1}H} NMR (162 MHz, CDCl$_3$): δ [ppm] = 29.1 (s, Eu-O=*P*Ph$_2$Ar), 19.3 (*trans*-(*P*Ph$_2$Ar)$_2$-PtCl$_2$), 13.3 (d, $^1J_{P,Pt}$ = 3682 Hz, *cis*-(*P*Ph$_2$Ar)$_2$-PtCl$_2$). – *cis*/*trans*-ratio approx. 30:1. Due to the low amount, no ^{195}Pt satellites are detected for the *trans*-species.

^{19}F NMR (377 MHz, CDCl$_3$): δ [ppm] = -79.8 (bs, C*F*$_3$)

IR (ATR): $\tilde{\nu}$ [cm^{-1}] = 3083 (w), 3059 (w), 3025 (m), 3001 (vw), 2925 (s), 2848 (w), 1601 (m), 1539 (vw), 1493 (m), 1452 (m), 1436 (m), 1406 (vw), 1376 (vw), 1309 (vw), 1203 (vw), 1182 (w), 1155 (vw), 1119 (vw), 1097 (w), 1069 (vw), 1029 (w), 907 (vw), 759 (m), 746 (m), 697 (vs), 540 (w).

Synthesis of Intermediate Structures

As described in the above section *'Synthesis of Heterometallic Eu(III)/Pt(II)-SCNPs'* the heterometallic SCNP synthesis can be performed by simultaneous addition of both Pt(II) and Eu(III) metal precursors. Therefore, the nanoparticle formation seems to be independent from the sequence of metal ion addition, due to the orthogonal coordination behavior of phosphine and phosphine oxides, allowing dual functionalization and single-chain collapse in one step.

To confirm the selective metal coordination of the two disparate ligand functionalities, phosphine and phosphine oxide, further experiments were performed. Hereby, terpolymer **$P_{P/Oxide}$** was individually reacted with the metal precursors [$PtCl_2$(cod)], [Eu(dbm)$_3$(H_2O)$_2$] and [Eu(tta)$_3$(H_2O)], yielding the functionalized polymers '**$P_{P/Oxide}$-$PtCl_2$**', '**$P_{P/Oxide}$-Eu(dbm)$_3$**' and '**$P_{P/Oxide}$-Eu(tta)$_3$**' (Scheme S4 and S5). Hereby, '**$P_{P/Oxide}$-$PtCl_2$**' is considered a SCNP structure (formally Pt(II)-SCNPs), whereas '**$P_{P/Oxide}$-Eu(dbm)$_3$**' and '**$P_{P/Oxide}$-Eu(tta)$_3$**' are considered merely metallopolymers. The isolation of these 'intermediate species' indicates a selective coordination behavior of platinum and europium towards phosphine and phosphine oxide, respectively.

Therefore, a phosphine oxide Eu(III) coordination can be realized either prior or subsequent to the Pt induced chain folding, resulting in an analogue Eu(III)-Pt(II)-SCNP system. The corresponding ^{1}H, ^{31}P{^{1}H} and ^{19}F NMR spectra of the 'intermediate structures' are depicted in Fig. S10 to S16.

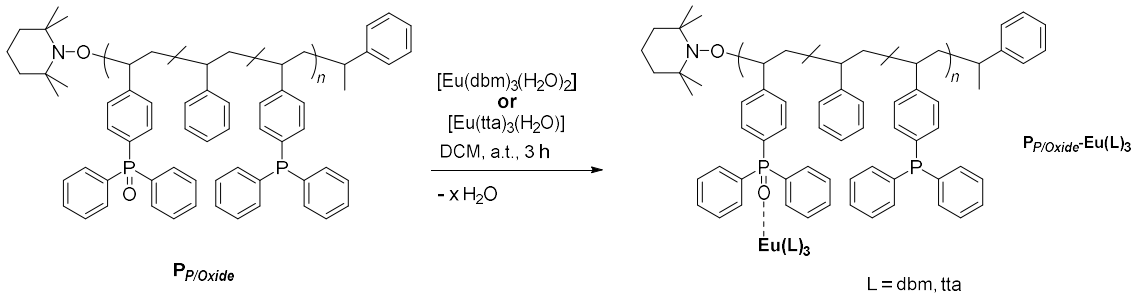

Scheme S4. Synthesis of metallopolymers **$P_{P/Oxide}$-Eu(dbm)$_3$** and **$P_{P/Oxide}$-Eu(tta)$_3$** applying the Eu(III) precursors [Eu(dbm)$_3$(H_2O)$_2$] and [Eu(tta)$_3$(H_2O)]. The respective europium species coordinates selectively to the phosphine oxide moieties of the polymer chains in a 1:1 metal-to-ligand ratio. The triarylphosphine moieties remain unaffected by the addition of europium.

$P_{P/Oxide}$ (50.0 mg, 7.90 µmol phosphine oxide functional groups, 15.8 µmol phosphine functional groups, 1.00 equiv.) was dissolved in 20.0 mL DCM and the complex [Eu(dbm)$_3$(H_2O)$_2$] (6.77 mg, 7.90 µmol, 1.00 equiv. with regards to the phosphine oxide moieties) was added subsequently. The solution was stirred for approximately 3 hours, and then concentrated under reduced pressure (to 1-2 mL). The solution was precipitated into cold MeOH, yielding the metallopolymer **$P_{P/Oxide}$-Eu(dbm)$_3$** after filtration.

Following the same reaction procedure, the metallopolymer **$P_{P/Oxide}$-Eu(tta)$_3$** was synthesized, applying the Eu(III) precursor complex [Eu(tta)$_3$(H_2O)].

SEC characterization: As described for the **Eu(III)/Pt(II)-SCNPs**, the linkages between Eu(III) and the phosphine oxide units in the polymer chains are not strong enough to withstand the conditions of SEC. Hence, an elugram similar to the one observed for terpolymer **$P_{P/Oxide}$** is observed.

$P_{P/Oxide}$-Eu(dbm)$_3$

^{1}H NMR (400 MHz, $CDCl_3$): δ [ppm] = 8.07–7.93 (m, Eu(dbm)$_3$-Ph), 7.69–6.10 (m, aromatic protons of all incorporated monomers and Eu(dbm)$_3$-Ph), 2.39–0.75 (m, aliphatic protons, backbone).

^{31}P{^{1}H} NMR (162 MHz, $CDCl_3$): δ [ppm] = 29.9 (s, Eu-O=*P*Ph$_2$Ar), -6.34 (s, *P*Ph$_2$Ar). – In comparison to $P_{P/Oxide}$, a decrease in integral value is observed for the resonance of the triarylphosphine oxide species (δ = 29.9 ppm). This is presumably caused by the coordination to the paramagnetic europium(III) cores. The triarylphosphine moieties are not affected by the addition of europium.

$P_{P/Oxide}$-Eu(tta)$_3$

^{1}H NMR (400 MHz, $CDCl_3$): δ [ppm] = 7.96–6.10 (m, aromatic protons of all incorporated monomers), 2.44–0.78 (m, aliphatic protons, backbone). – Due to the paramagnetic properties of the Eu(III) species the proton resonances for the thenoyltrifluoroacetonate (tta) ligands cannot be resolved and overlay partially with the aromatic proton resonances of the terpolymer.

^{31}P{^{1}H} NMR (162 MHz, $CDCl_3$): δ [ppm] = 29.2 (s, Eu-O=*P*Ph$_2$Ar), -6.22 (s, *P*Ph$_2$Ar). – In comparison to $P_{P/Oxide}$, a decrease in integral value is observed for the resonance of the triarylphosphine oxide species (δ = 29.2 ppm). This is presumably caused by the coordination to the paramagnetic europium(III) cores. The triarylphosphine moieties are not affected by the addition of europium.

^{19}F NMR (377 MHz, $CDCl_3$): δ [ppm] = -79.9 (bs, C*F*$_3$)

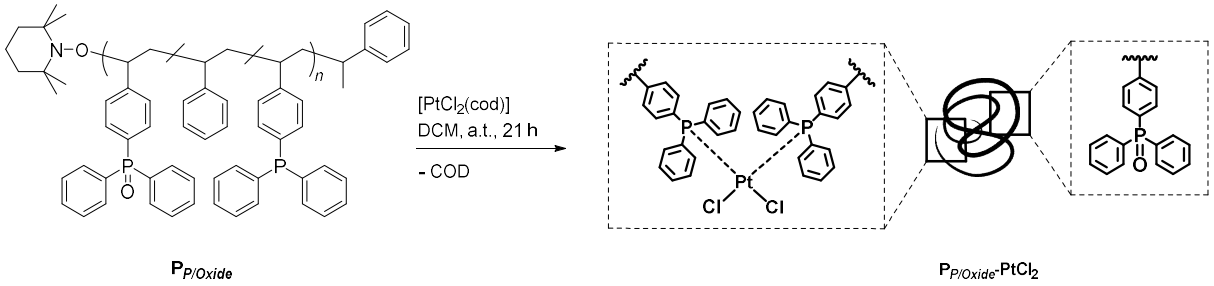

$P_{P/Oxide}$ $P_{P/Oxide}$-$PtCl_2$

Scheme S5. Synthesis of $P_{P/Oxide}$-$PtCl_2$ (formally Pt(II)-SCNPs) applying terpolymer $P_{P/Oxide}$ and the metal precursor [$PtCl_2$(cod)]. The platinum species coordinates selectively to the phosphine ligands of the polymer chains in a 2:1 ligand-metal ratio, resulting in a single-chain collapse. The triarylphosphine oxide moieties remain unaffected by the addition of platinum.

^{1}H NMR (400 MHz, $CDCl_3$): δ [ppm] = 7.92–6.13 (m, aromatic protons of all incorporated monomers), 2.34–0.57 (m, aliphatic protons, backbone).

^{31}P{^{1}H} NMR (162 MHz, $CDCl_3$): δ [ppm] = 29.0 (s, O=*P*Ph$_2$Ar), 19.3 (*trans*-(*P*Ph$_2$Ar)$_2$-$PtCl_2$), 13.3 (d, $^1J_{P,Pt}$ = 3686 Hz, *cis*-(*P*Ph$_2$Ar)$_2$-$PtCl_2$). – *cis*/*trans*-ratio approx. 30:1. Due to the low amount, no ^{195}Pt satellites are detected for the *trans*-species. The phosphine oxide moieties are not affected by the platinum addition.

Further remarks:

Additionally, the sole coordination of [Eu(dbm)$_3$] to a triarylphosphine oxide containing copolymer (styrene based) was performed at high concentrations. Under these reaction conditions a network formation would occur in case of a 2:1 ligand to Eu(III) coordination. However, neither any solubility issues nor problems in filtering of the dissolved compound occurred. For this reason, an Eu(III) coordination ratio of 1:1 was assumed for both heterometallic SCNP systems as well as **$P_{P/Oxide}$-Eu(dbm)$_3$** and **$P_{P/Oxide}$-Eu(tta)$_3$**.

This assumption was further confirmed by DOSY NMR measurements. Hereby, analysis of '**$P_{P/Oxide}$-Eu(dbm)$_3$**' resulted in a hydrodynamic radius of r_H = 11.2 nm. This represents a significant increase in comparison to terpolymer **$P_{P/Oxide}$** (r_H = 8.0 nm). Hence, it can be excluded that the Eu species induces any chain compaction, and coordinates in a 1:1 metal-to-ligand ratio to the phosphine oxide ligands of **$P_{P/Oxide}$**. On the other hand, a significantly smaller hydrodynamic radius of r_H = 1.9 nm was determined for the **Eu$_{(dbm)}$(III)/Pt(II)-SCNPs**, as expected for a chain compaction.

For more details refer to the section *'DOSY Measurements'* in the Supporting Information (see below).

Original Data

NMR spectra

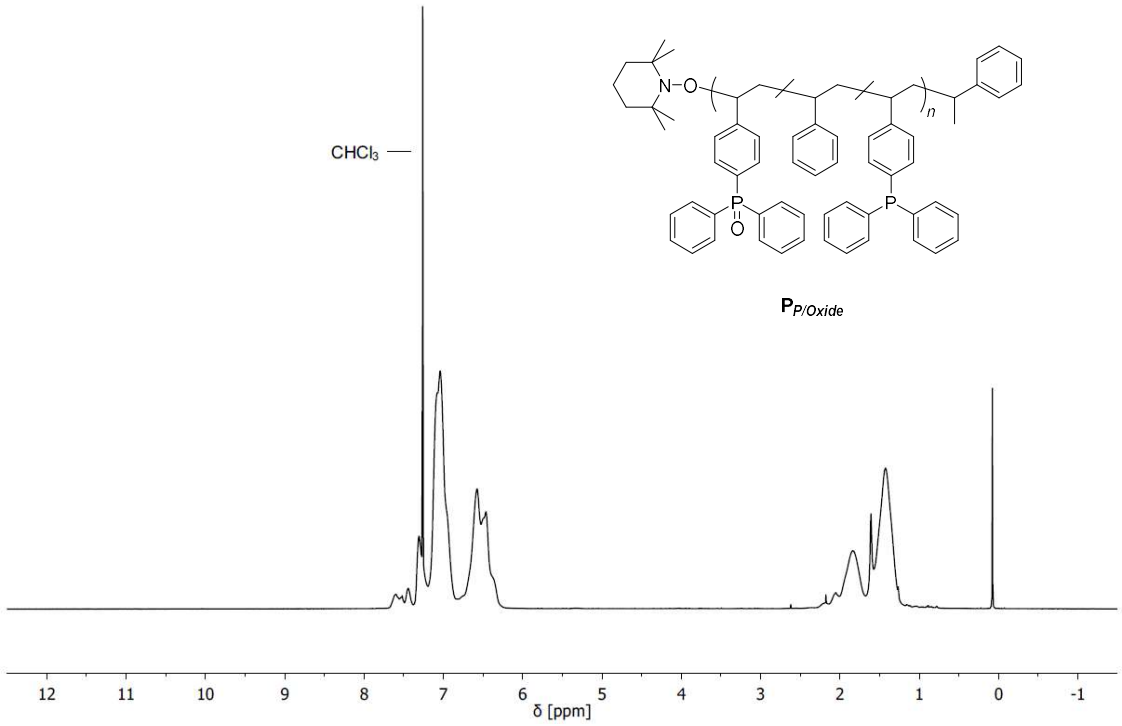

Fig. S1. ^{1}H NMR spectrum of $P_{P/Oxide}$ in $CDCl_3$ (400 MHz; 298 K).

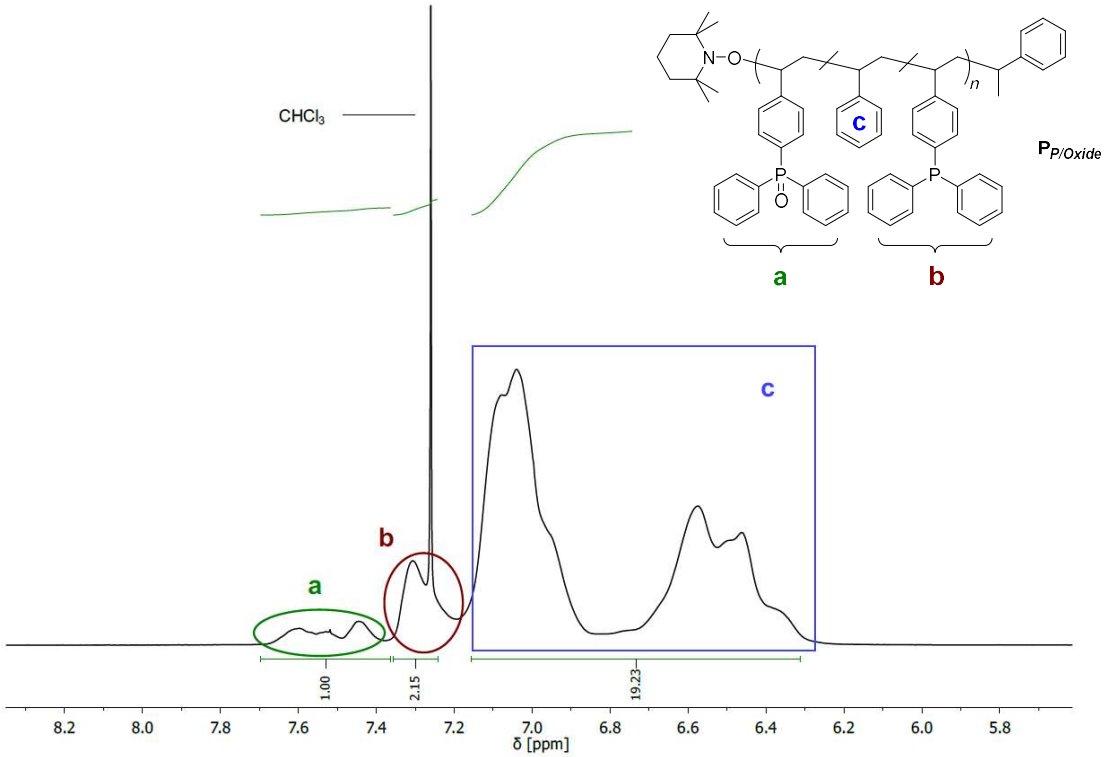

Fig. S2. Assignment and integration of the aromatic resonances of $P_{P/Oxide}$ in the ^{1}H NMR spectrum. Regarding the tolerable distinction of triarylphosphine and triarylphosphine oxide resonances (a and b), refer to Fig. S17 and S19.

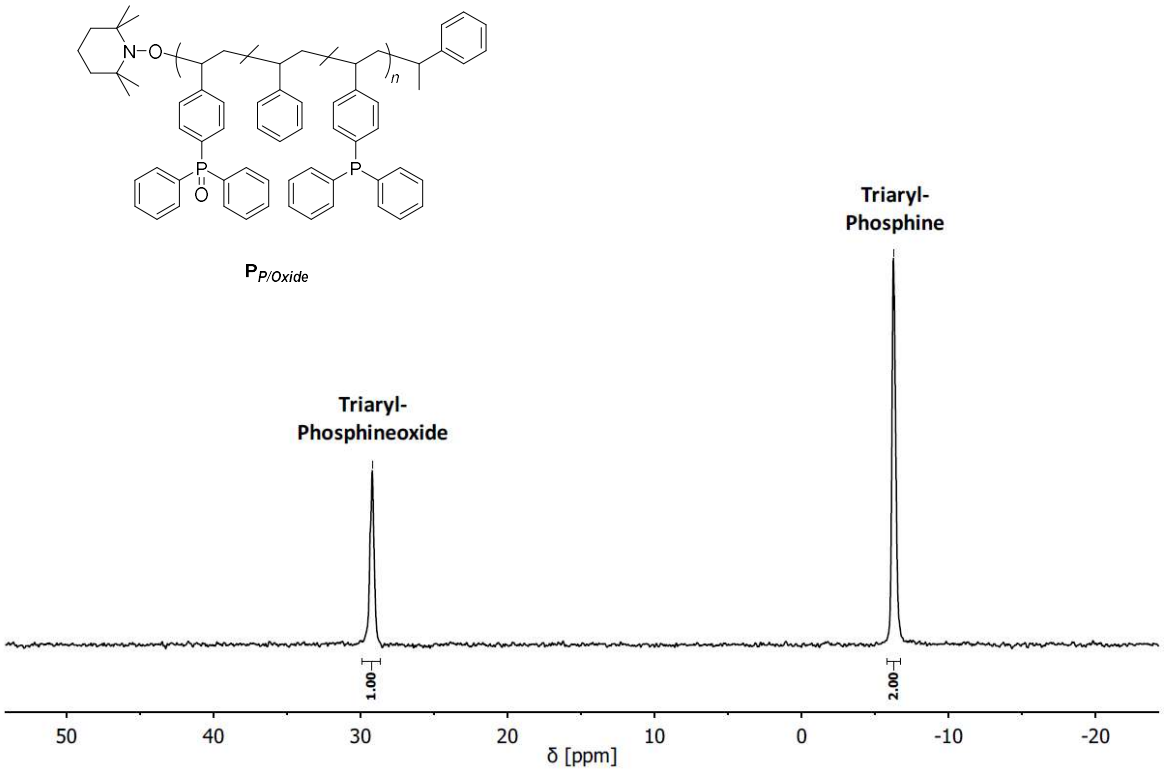

Fig. S3. $^{31}P\{^{1}H\}$ NMR spectrum of **$P_{P/Oxide}$** in $CDCl_3$ (162 MHz; 298 K).

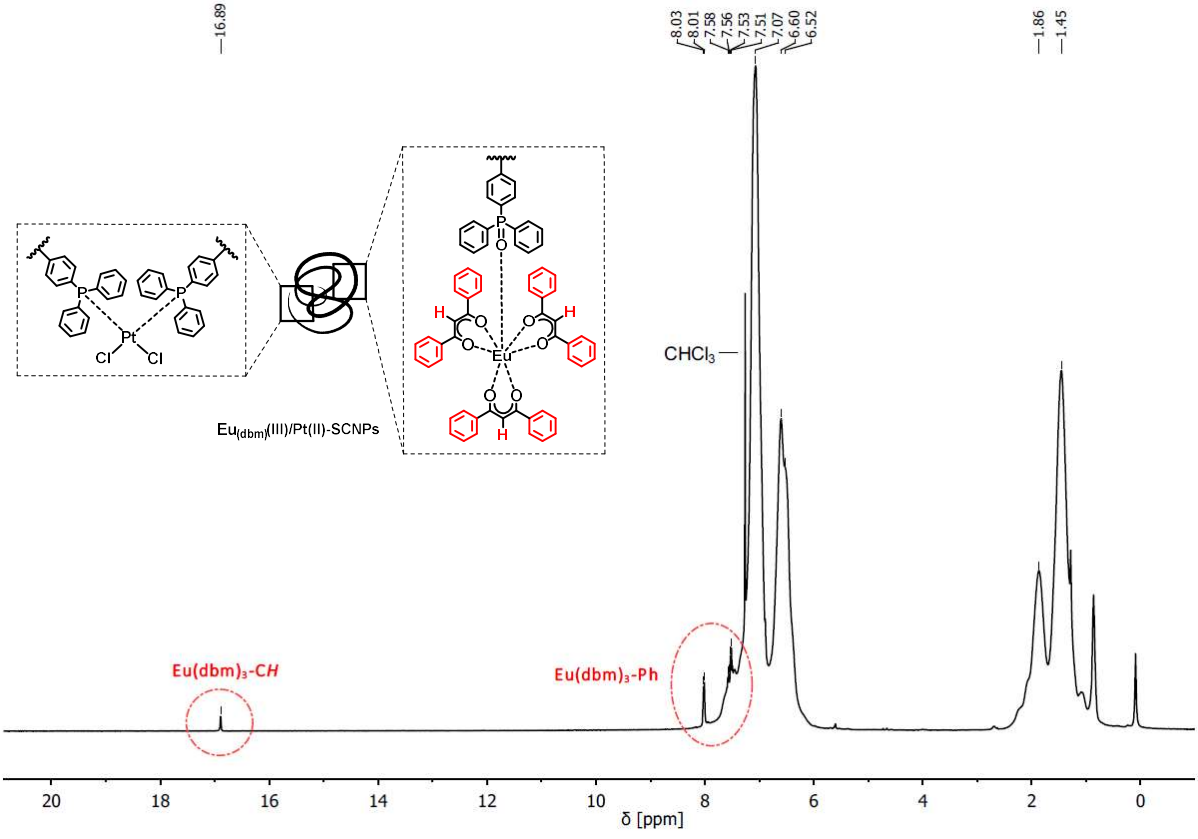

Fig. S4. ^{1}H NMR spectrum of **$Eu_{(dbm)}$(III)/Pt(II)-SCNPs** in $CDCl_3$ (400 MHz; 298 K). The proton resonances of the $[Eu(dbm)_3]$ moieties are marked with red circles.

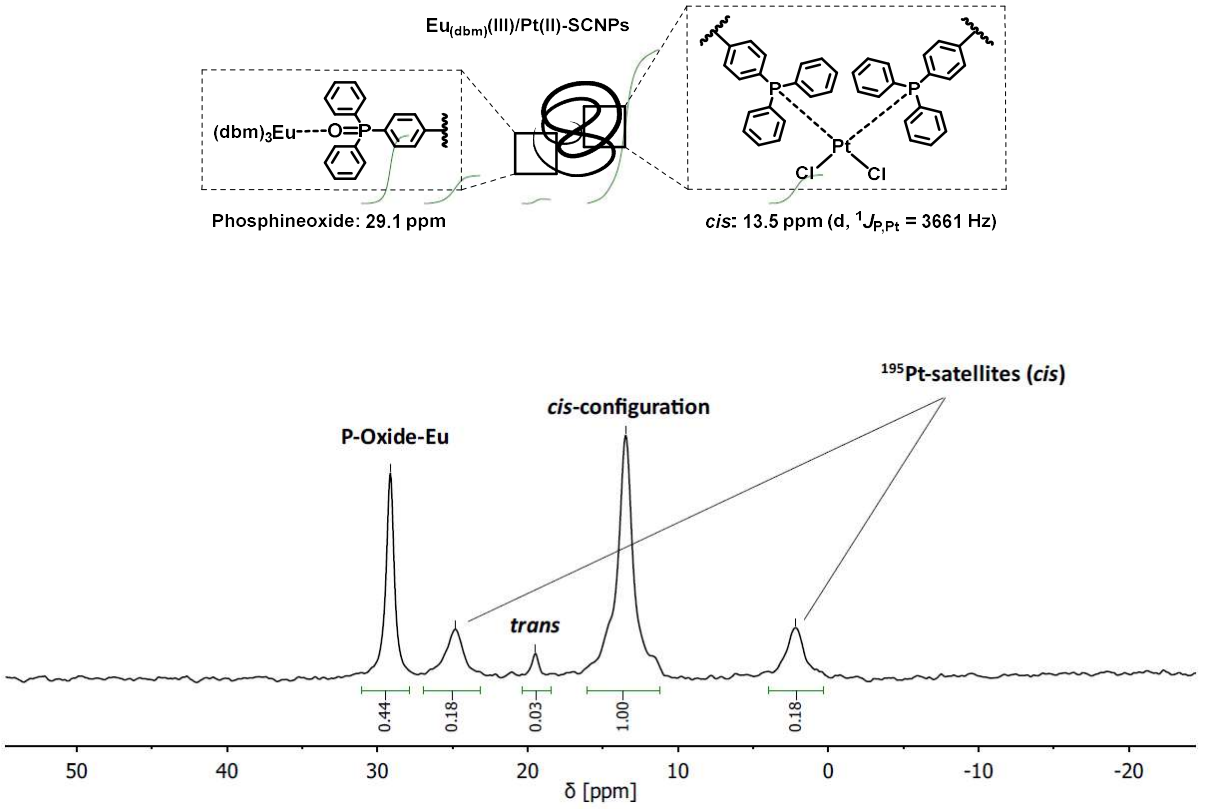

Fig. S5. $^{31}P\{^{1}H\}$ NMR spectrum of **$Eu_{(dbm)}$(III)/Pt(II)-SCNPs** in $CDCl_3$ (162 MHz; 298 K). Comparing the integral values of the resonances for the *cis*- and *trans*-species, a ratio of approx. 30:1 (*cis*/*trans*) is calculated (within the boundaries of NMR spectroscopy).

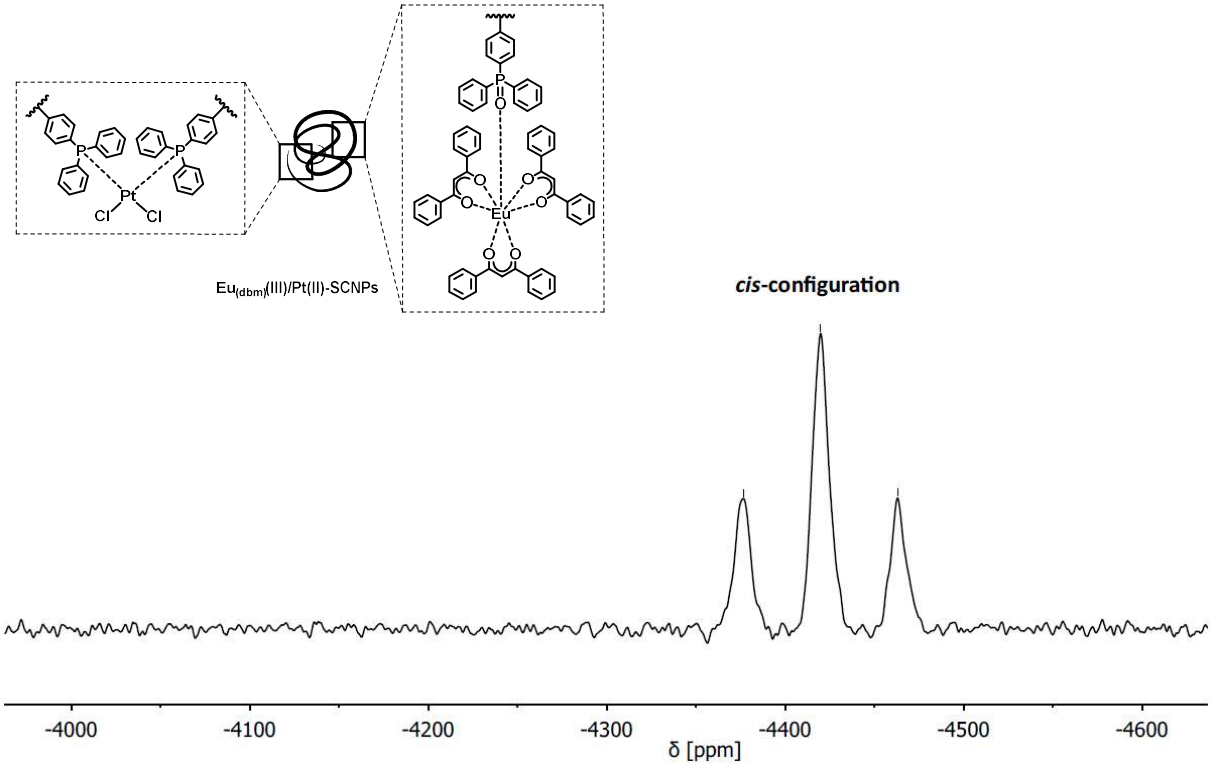

Fig. S6. ^{195}Pt NMR spectrum of **$Eu_{(dbm)}$(III)/Pt(II)-SCNPs** in $CDCl_3$ (86 MHz; 298 K).

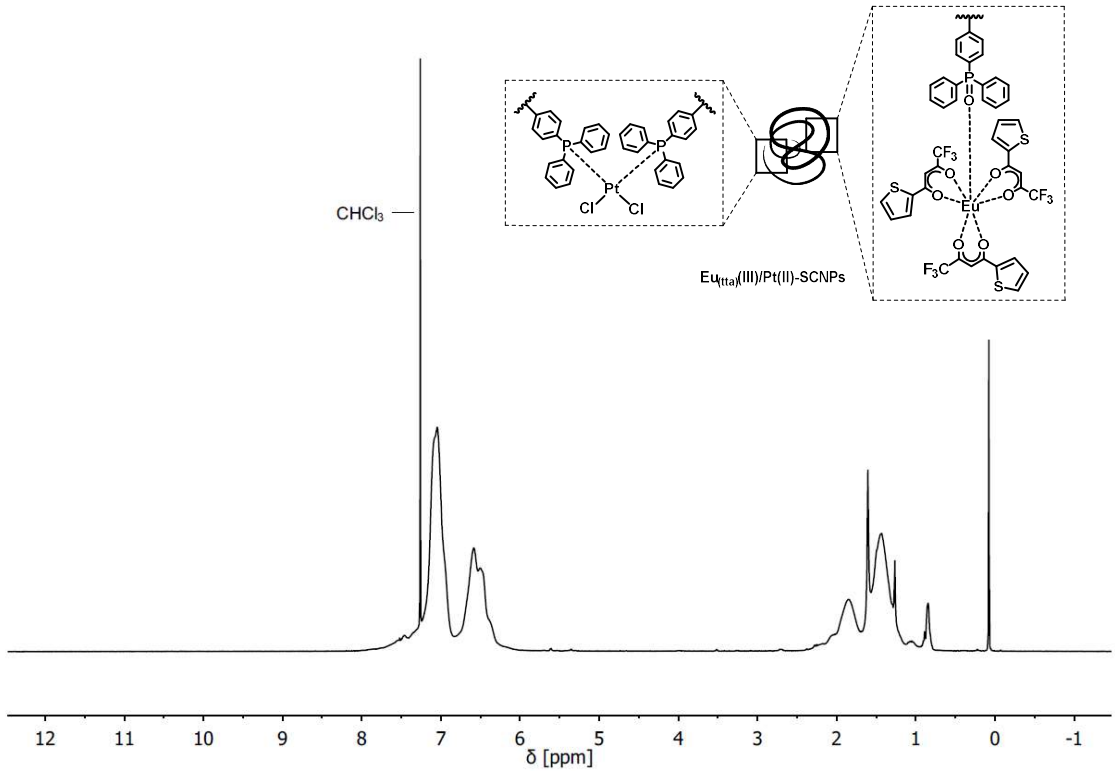

Fig. S7. ^{1}H NMR spectrum of **$Eu_{(tta)}$(III)/Pt(II)-SCNPs** in $CDCl_3$ (400 MHz; 298 K).

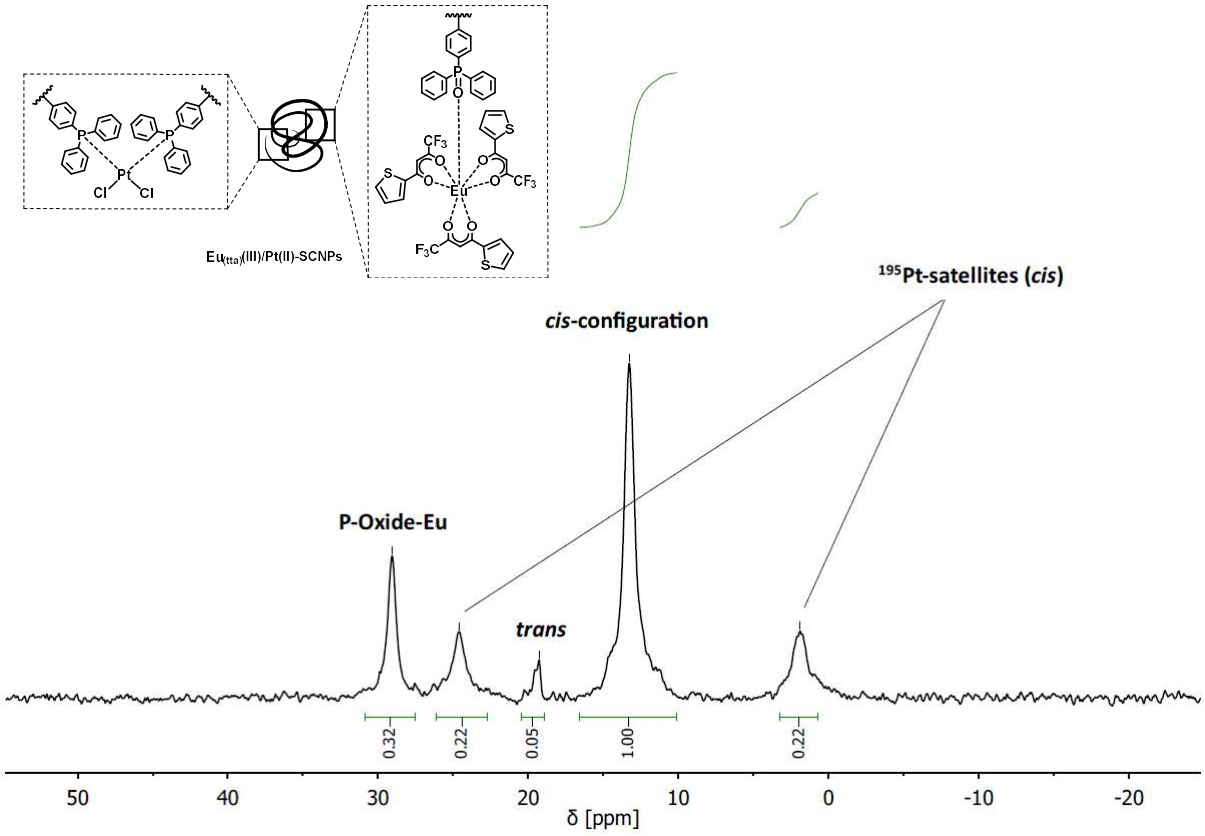

Fig. S8. $^{31}P\{^{1}H\}$ NMR spectrum of **$Eu_{(tta)}$(III)/Pt(II)-SCNPs** in $CDCl_3$ (162 MHz; 298 K).

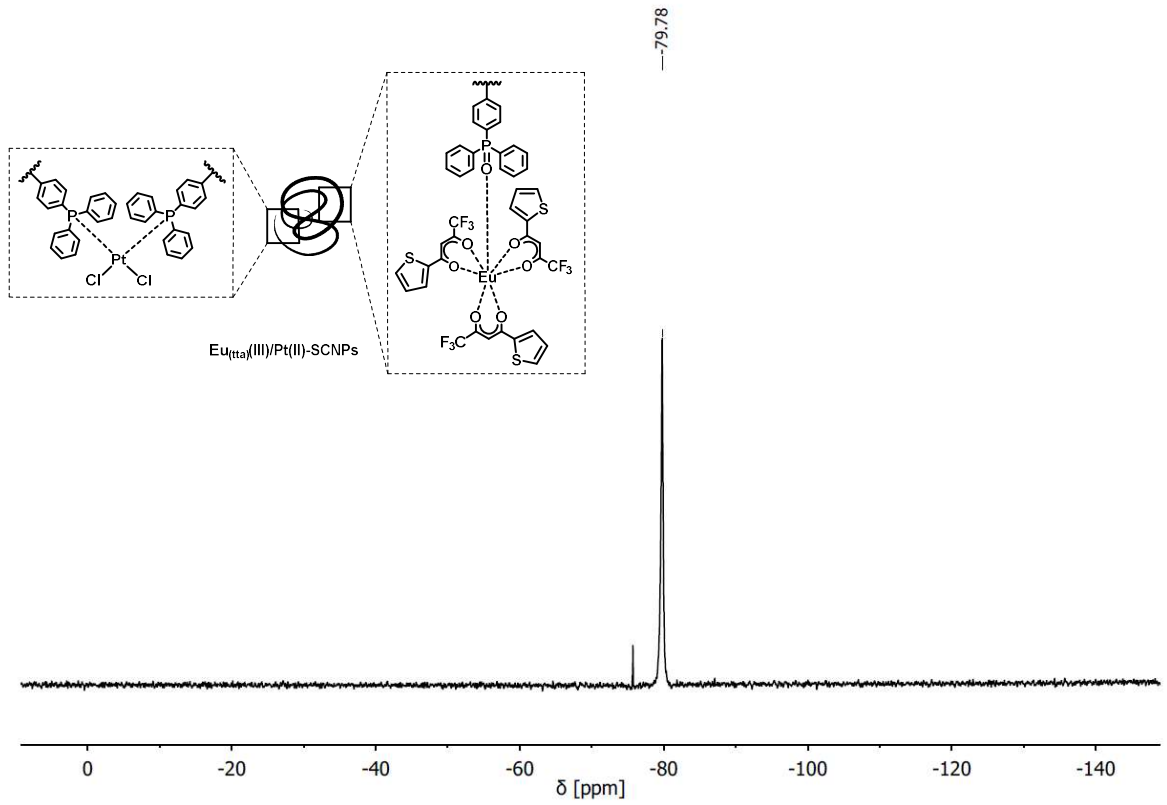

Fig. S9. ^{19}F NMR spectrum of **$Eu_{(tta)}$(III)/Pt(II)-SCNPs** in $CDCl_3$ (377 MHz; 298 K).

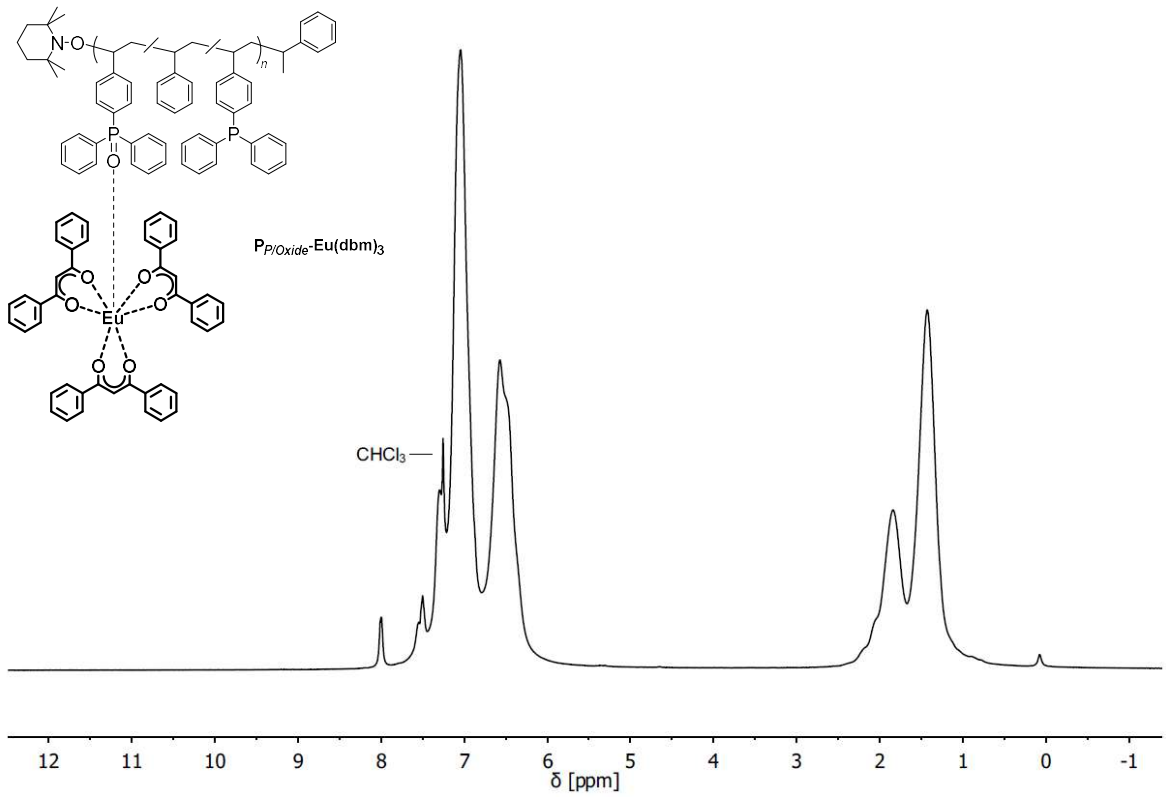

Fig. S10. ^{1}H NMR spectrum of **$P_{P/Oxide}$-Eu(dbm)$_3$** in $CDCl_3$ (400 MHz; 298 K).

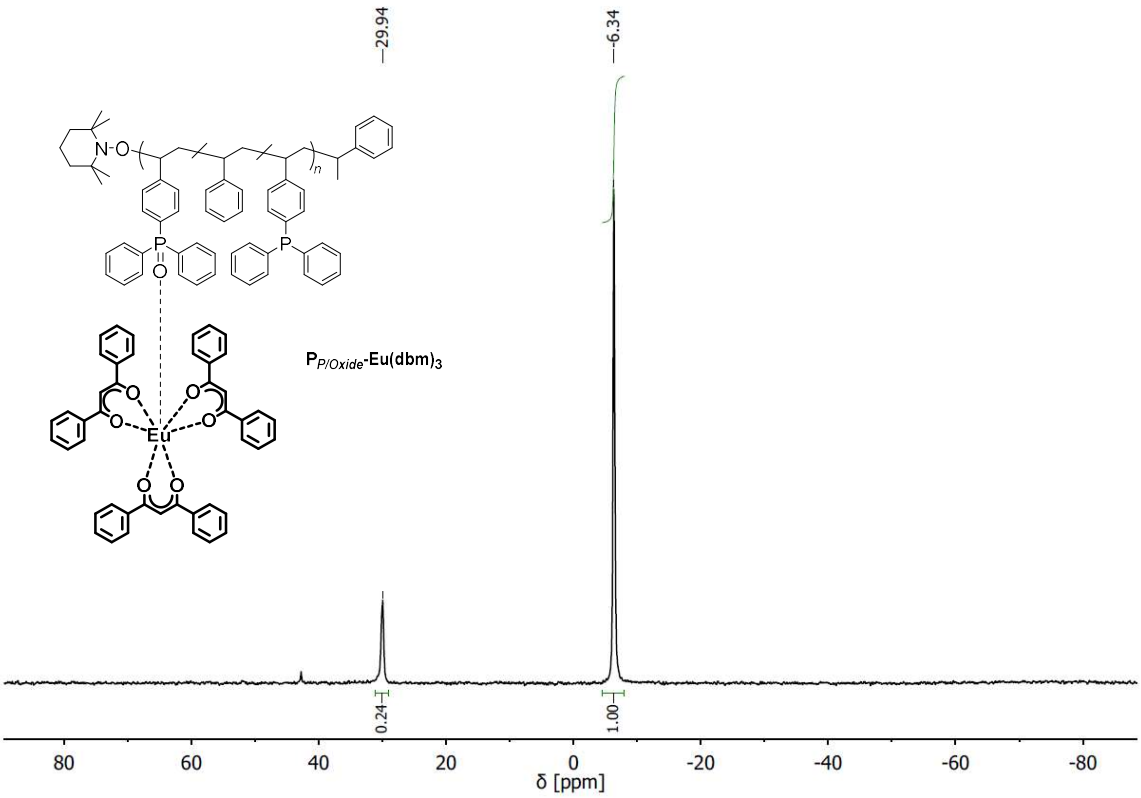

Fig. S11. $^{31}P\{^1H\}$ NMR spectrum of **$P_{P/Oxide}$-Eu(dbm)$_3$** in $CDCl_3$ (162 MHz; 298 K). In comparison to **$P_{P/Oxide}$**, a decrease in integral value is observed for the triarylphosphine oxide resonance (δ = 29.9 ppm). This is presumably caused by the coordination to the paramagnetic europium(III) cores. A similar effect is observed in the $^{31}P\{^1H\}$ NMR spectra of **$P_{P/Oxide}$-Eu(tta)$_3$** (Fig. S13), **$Eu_{(dbm)}$(III)/Pt(II)-SCNPs** (Fig. S5) and **$Eu_{(tta)}$(III)/Pt(II)-SCNPs** (Fig. S8).

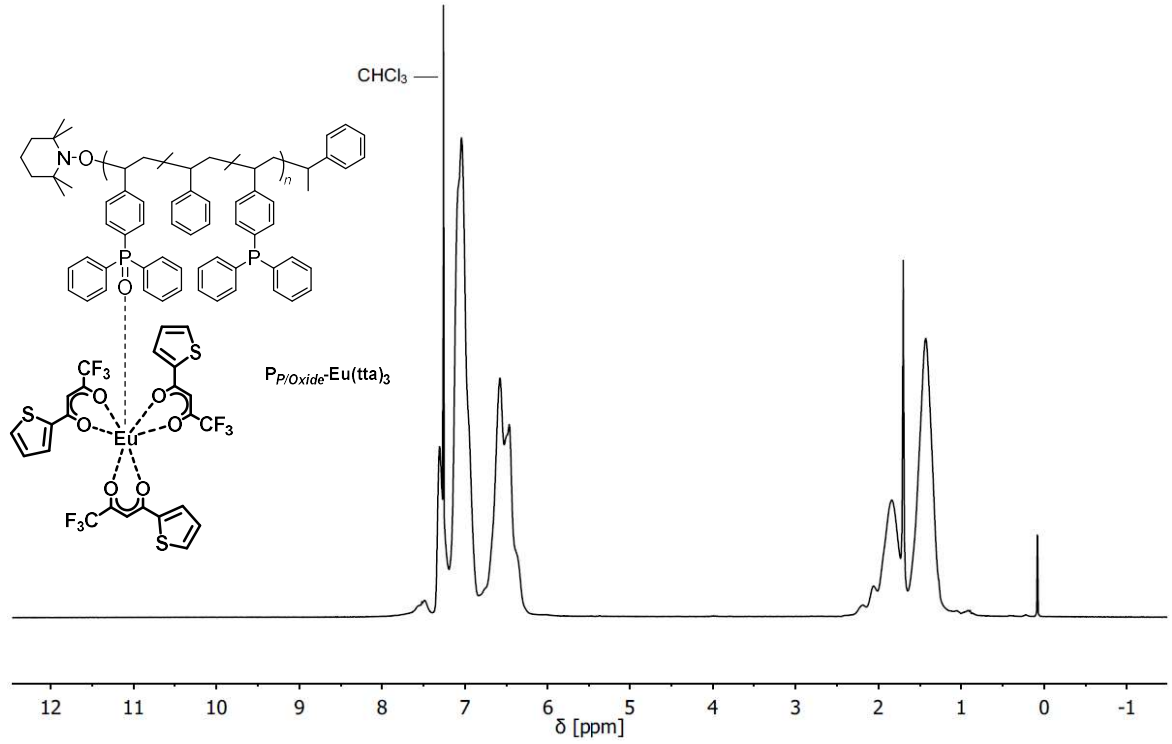

Fig. S12. ^1H NMR spectrum of **$P_{P/Oxide}$-Eu(tta)$_3$** in $CDCl_3$ (400 MHz; 298 K).

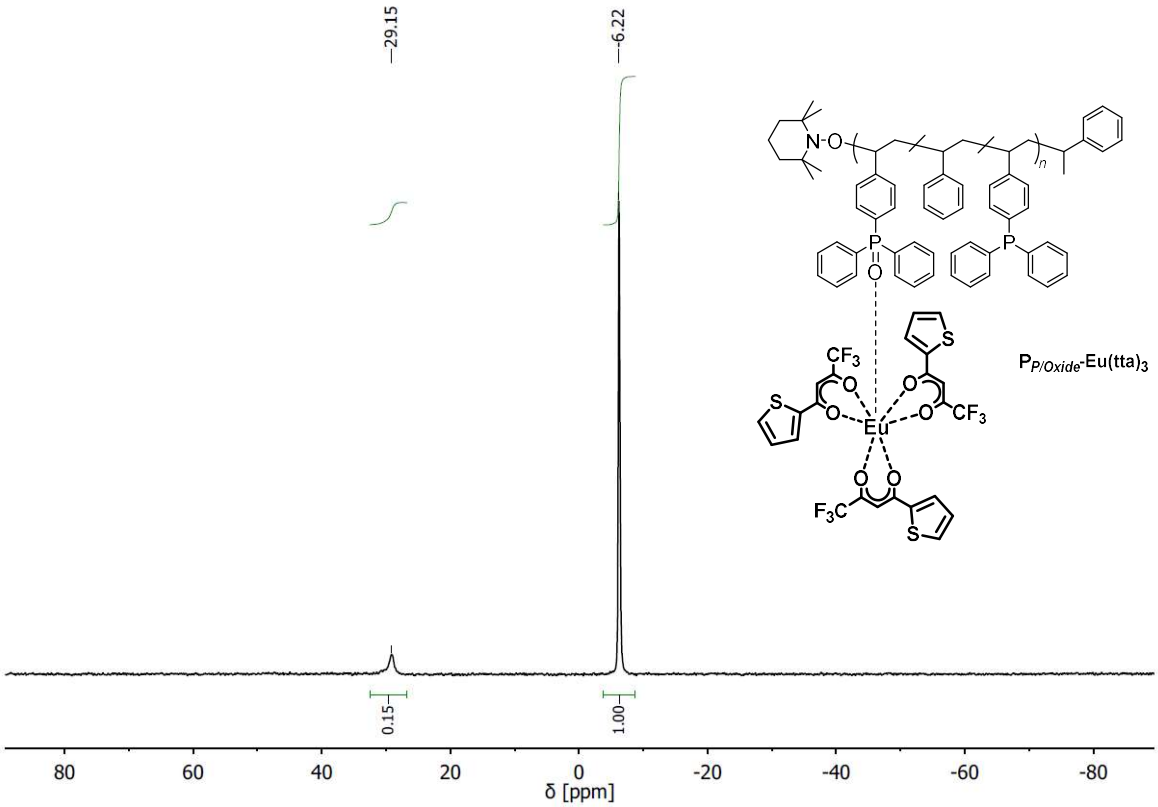

Fig. S13. $^{31}P\{^1H\}$ NMR spectrum of **$P_{P/Oxide}$-Eu(tta)$_3$** in $CDCl_3$ (162 MHz; 298 K). In comparison to **$P_{P/Oxide}$**, a decrease in integral value is observed for the triarylphosphine oxide resonance (δ = 29.2 ppm). This is presumably caused by the coordination to the paramagnetic europium(III) cores. A similar effect is observed in the $^{31}P\{^1H\}$ NMR spectra of **$P_{P/Oxide}$-Eu(dbm)$_3$** (Fig. S11), **Eu$_{(dbm)}$(III)/Pt(II)-SCNPs** (Fig. S5) and **Eu$_{(tta)}$(III)/Pt(II)-SCNPs** (Fig. S8).

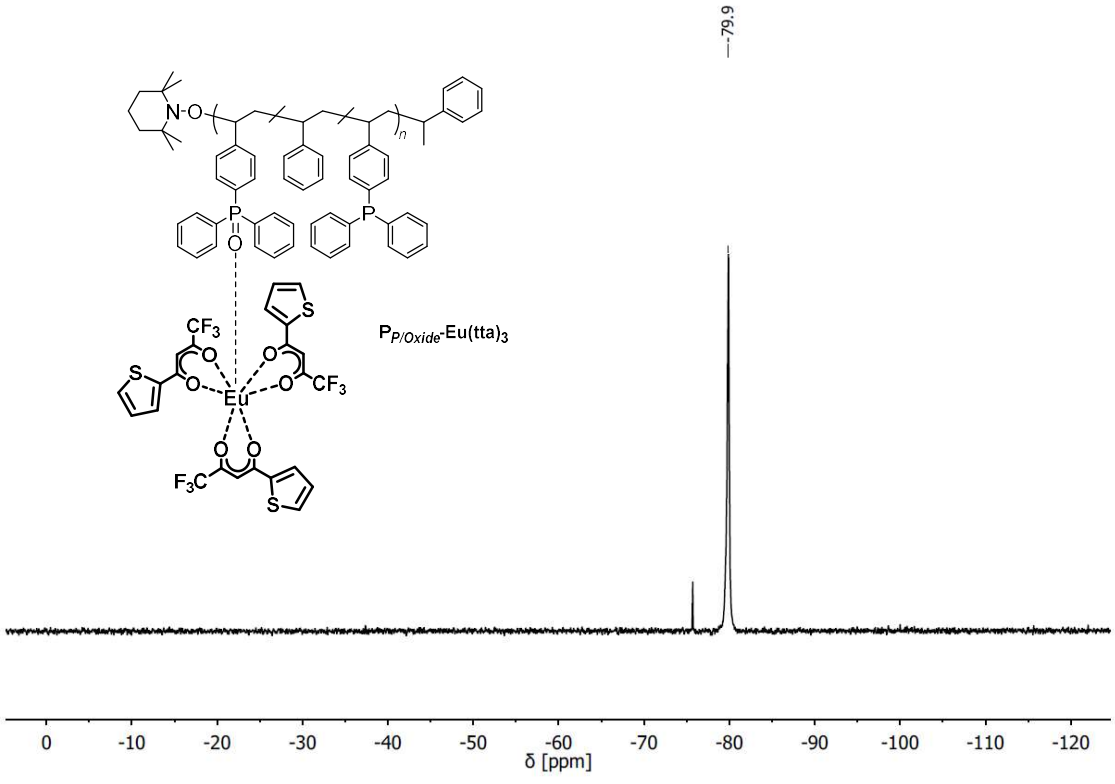

Fig. S14. ^{19}F NMR spectrum of **$P_{P/Oxide}$-Eu(tta)$_3$** in $CDCl_3$ (377 MHz; 298 K).

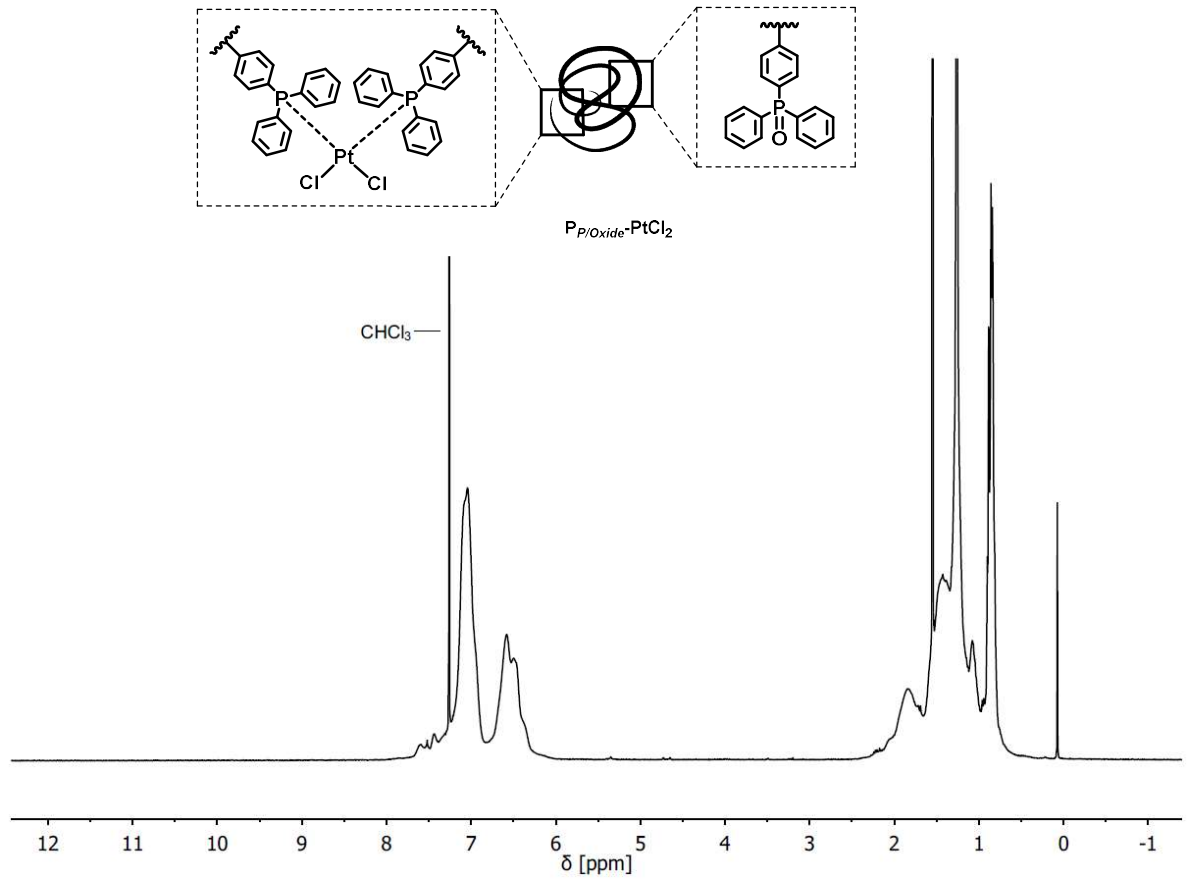

Fig. S15. ^{1}H NMR spectrum of $P_{P/Oxide}$-$PtCl_2$ (formally Pt(II)-SCNPs) in $CDCl_3$ (400 MHz; 298 K).

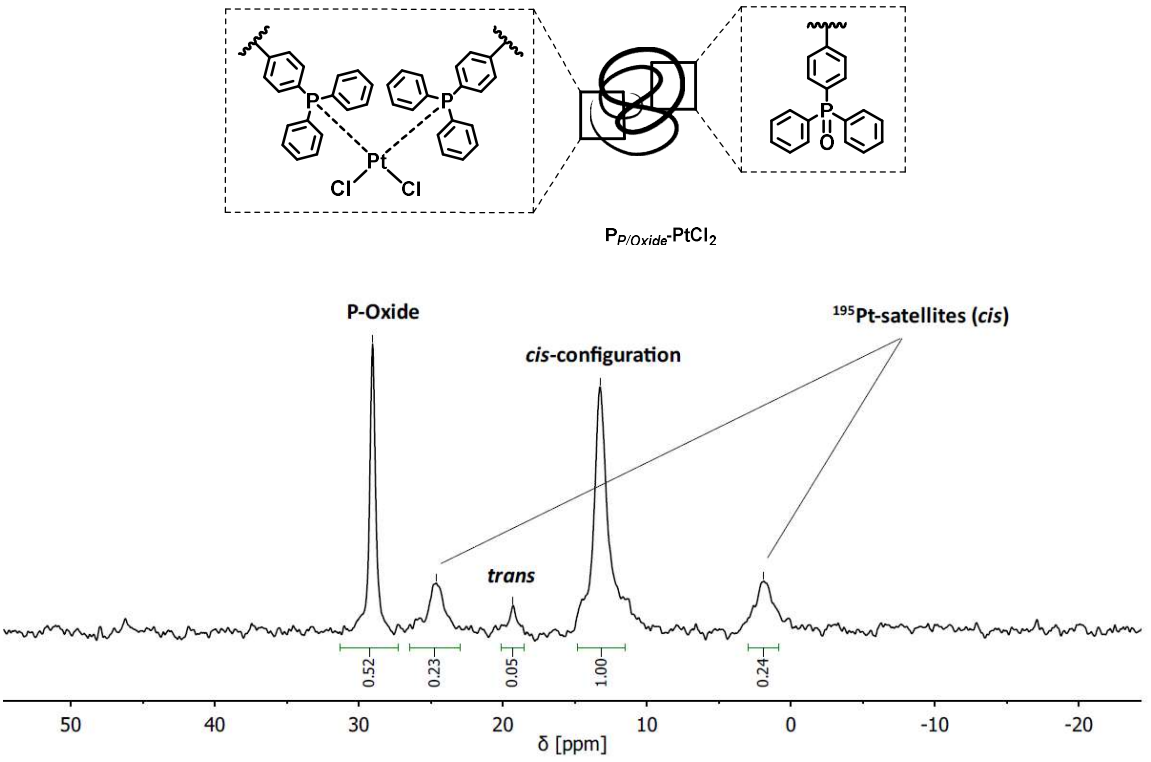

Fig. S16. $^{31}P\{^{1}H\}$ NMR spectrum of $P_{P/Oxide}$-$PtCl_2$ (formally Pt(II)-SCNPs) in $CDCl_3$ (162 MHz; 298 K). The triarylphosphine oxide resonance remains unaffected by the addition of platinum.

Additional NMR experiments

Further NMR experiments were conducted, aiming for a more accurate evaluation of the NMR data with regards to terpolymer **$P_{P/Oxide}$**. Specifically, an investigation regarding a resonance assignment of the two incorporated ligand systems (triarylphosphine and triarylphosphine oxide) in the terpolymer proved to be necessary. Therefore, ^{1}H and $^{31}P\{^{1}H\}$ NMR spectra of the molecular compounds triphenylphosphine and triphenylphosphine oxide were recorded (Fig. S17 and S18). Additionally, styrene-based copolymers containing merely a triarylphosphine (**P_P**)[4] or triarylphosphine oxide (**P_{Oxide}**) functionalization were investigated by NMR spectroscopy (Fig. S19 and S20) and compared with regards to terpolymer **$P_{P/Oxide}$**.

In addition, $^{31}P\{^{1}H\}$ NMR spectra of the terpolymer **$P_{P/Oxide}$**, applying bis(diphenylphosphino)methane (DPPM) as an external standard, were recorded. Hence, a more accurate determination regarding the quantitative amounts of triarylphosphine and triarylphosphine oxide moieties in **$P_{P/Oxide}$** was achieved. Hereby, 19.7 mg of the terpolymer **$P_{P/Oxide}$** and 5.3 mg of bis(diphenylphosphino)methane were dissolved in 0.5 mL $CDCl_3$. Evaluation resulted in 0.17 mmol phosphine oxide species and 0.35 mmol phosphine species per 1 g of terpolymer **$P_{P/Oxide}$** (refer to Fig. S21).

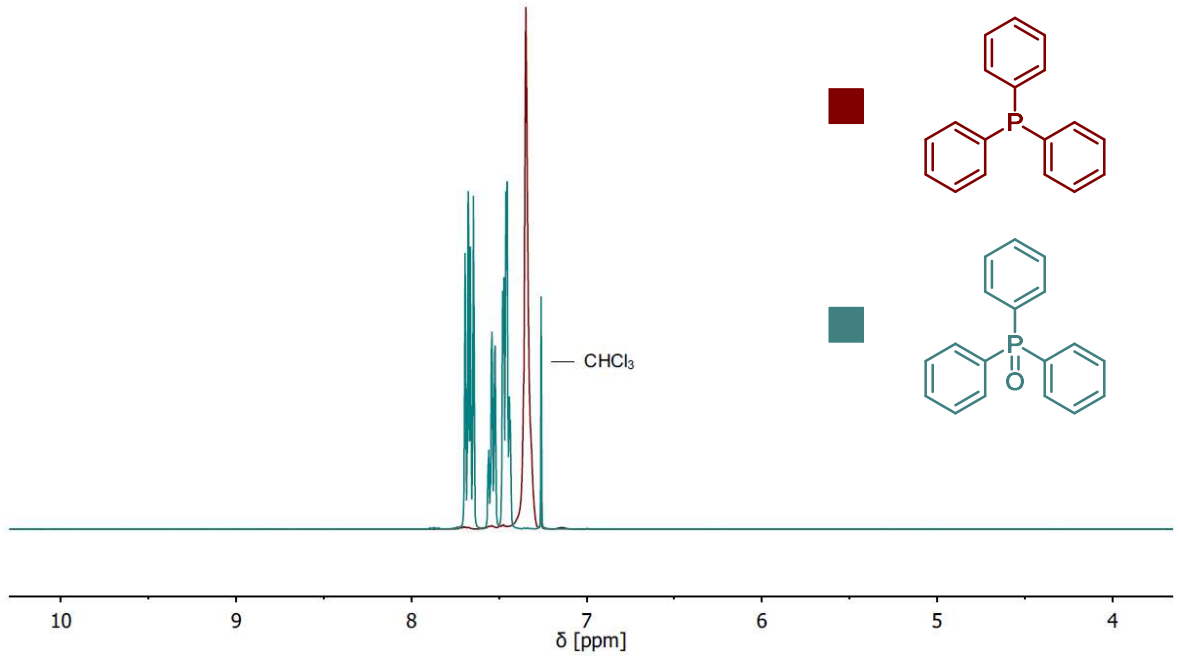

Fig. S17. Overlay ^{1}H NMR spectra of triphenylphosphine (red) and triphenylphosphine oxide (green) in $CDCl_3$ (400 MHz; 298 K), depicting the aromatic region. The spectra indicate that the compounds can be distinguished, with regards to their aromatic proton resonances. Hereby, the resonances of triphenylphosphine oxide are downfield shifted compared to triphenylphosphine.

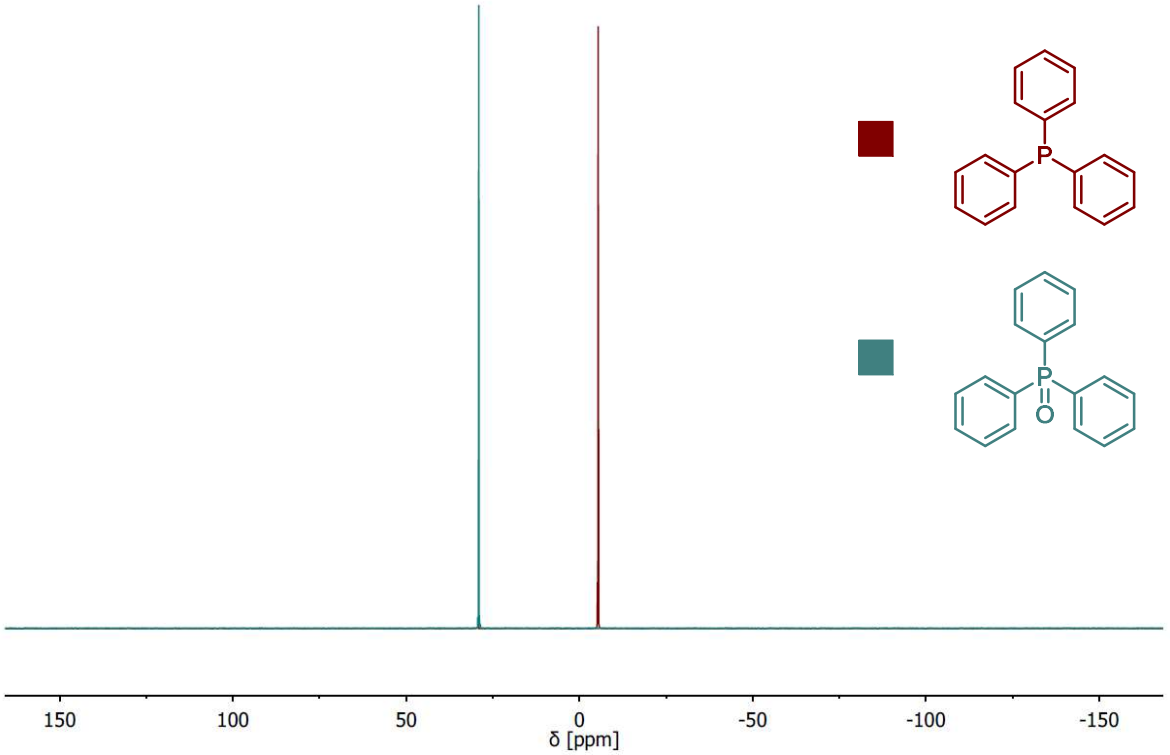

Fig. S18. Overlay $^{31}P\{^{1}H\}$ NMR spectra of triphenylphosphine (red) and triphenylphosphine oxide (green) in $CDCl_3$ (162 MHz; 298 K). The respective resonances match with the chemical shift observed in the terpolymer $\mathbf{P_{P/Oxide}}$ (refer to Fig. S3).

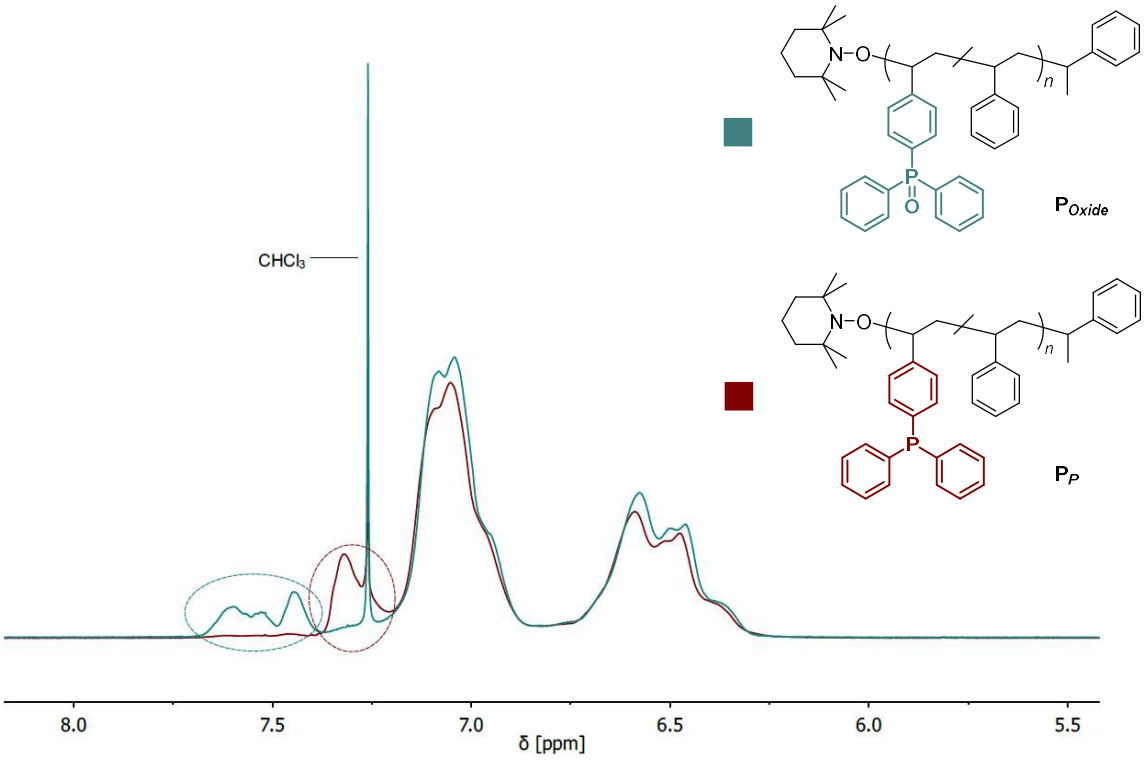

Fig. S19. Overlay ^{1}H NMR spectra of styrene-based copolymers, exhibiting either triarylphosphine ($\mathbf{P_P}$, red)[4] or triarylphosphine oxide ($\mathbf{P_{Oxide}}$, green) moieties (functionalization between 2-5 mol%), measured in $CDCl_3$ (400 MHz; 298 K). Merely the aromatic region is depicted. The spectra indicate that the aromatic proton resonances of triarylphosphine (red) or triarylphosphine oxide (green) moieties can be distinguished to a certain degree. Thus, a distinction of both species in the ^{1}H NMR spectrum of terpolymer $\mathbf{P_{P/Oxide}}$ seems reasonable within a certain error margin (refer to Fig. S2).

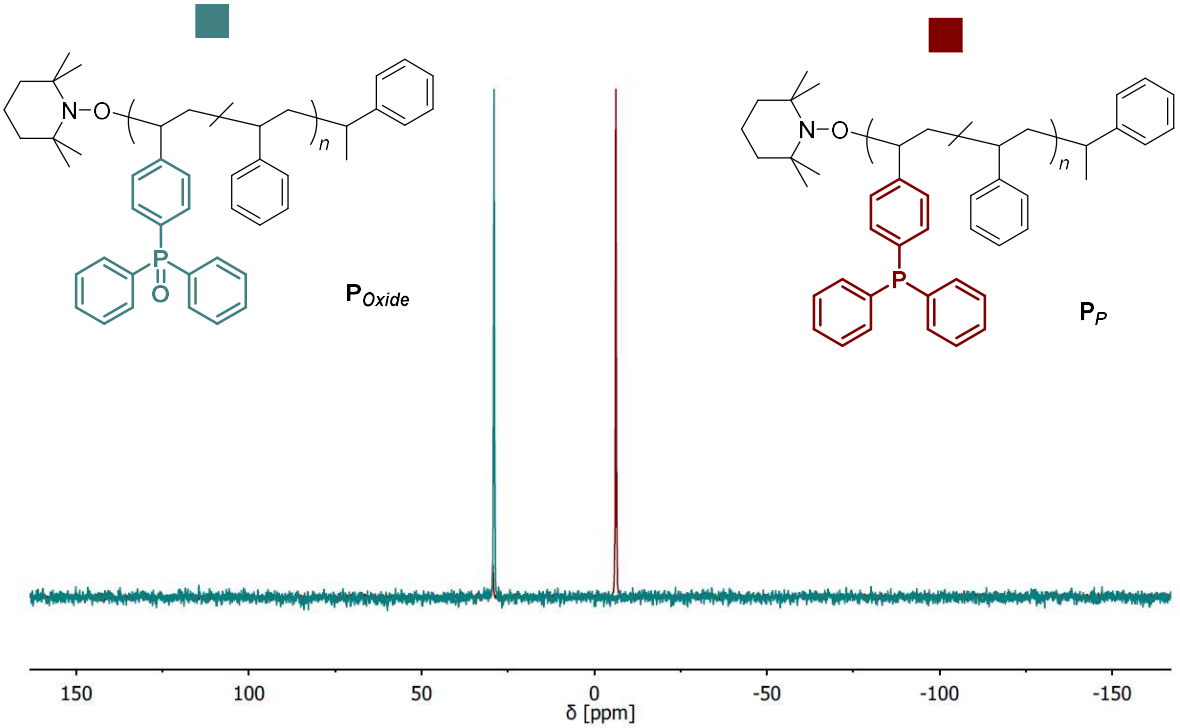

Fig. S20. Overlay $^{31}P\{^{1}H\}$ NMR spectra of styrene-based copolymers, exhibiting either triarylphosphine ($\mathbf{P_P}$, red)[4] or triarylphosphine oxide ($\mathbf{P_{Oxide}}$, green) moieties (functionalization between 2-5 mol%), measured in $CDCl_3$ (162 MHz; 298 K). The respective resonances match with the chemical shift observed in the terpolymer $\mathbf{P_{P/Oxide}}$ (refer to Fig. S3).

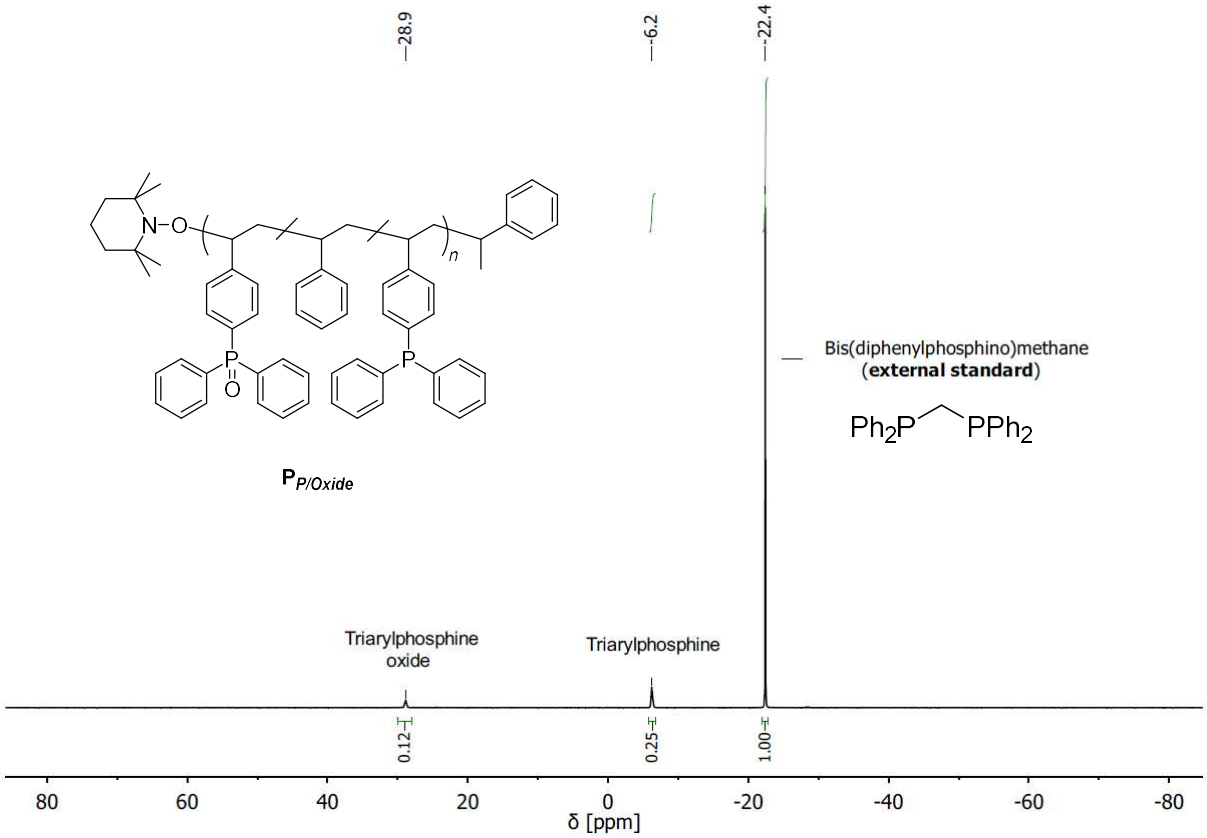

Fig. S21. $^{31}P\{^{1}H\}$ NMR spectrum of terpolymer $P_{P/Oxide}$ with the addition of bis(diphenylphosphino)methane as an external standard. The spectrum was measured in $CDCl_3$ (162 MHz; 298 K). Hereby, 19.7 mg of the terpolymer $P_{P/Oxide}$ and 5.3 mg of bis(diphenylphosphino)methane were dissolved in 0.5 mL $CDCl_3$. Evaluation resulted in 0.17 mmol phosphine oxide species and 0.35 mmol phosphine species per 1 g of terpolymer $P_{P/Oxide}$. Weighing errors as well as the purity of bis(diphenylphosphino)methane (97 %) need to be considered.

DOSY Measurements

Molecules are distinguished according to their diffusion coefficient, which correlates with their hydrodynamic radius (R_h). Terpolymer **P$_{P/Oxide}$**, **Eu$_{(dbm)}$(III)/Pt(II)-SCNPs** and metallopolymer **P$_{P/Oxide}$-Eu(dbm)$_3$** were analysed in $CDCl_3$ (c ~ 10-15 mg / 0.6 mL), employing a dynamic viscosity of η = 0.0005418 $\frac{N}{m^2}s$ (at 298.15 K).[5] Calculations of the hydrodynamic radii were carried out, applying the Stokes-Einstein Equation.

$$Stokes-Einstein\ Equation: \qquad D = \frac{k_B \cdot T}{6\pi \cdot \eta \cdot R_h} \;\; ; \;\; R_h = \frac{k_B \cdot T}{6\pi \cdot \eta \cdot \mathrm{D}}$$

$$k_B = 1.38 \cdot \frac{10^{-23} J}{K}; \quad T = 298.15\,K\,; \quad \eta(CDCl_3) = 0.5418\,cP = 0.5418\,mPa \cdot s\ (at\ 298.15\,K)$$

$$1\,Pa = 1\frac{N}{m^2}\,; \quad 1\,J = 1\,N \cdot m$$

$$R_h = \frac{1.38 \cdot 10^{-23}\frac{J}{K} \cdot 298.15\,K}{6\pi \cdot 0.0005418\frac{N}{m^2}s} \cdot \frac{1}{D}$$

$$R_h = \frac{4.115 \cdot 10^{-21} Jm^2}{0.0102127\ \mathrm{Ns}} \cdot \frac{1}{D}$$

$$R_h = 4.029 \cdot 10^{-19}\frac{m^3}{s} \cdot \frac{1}{D}$$

P$_{P/Oxide}$: $$D_{av.} = 5.01\ \cdot 10^{-11}\frac{m^2}{s};\ (averaged\ seven\ values)$$

$$R_h = 8.04 \cdot 10^{-9}\,m = 8.04\ \mathrm{nm}$$

Eu$_{(dbm)}$(III)/Pt(II)-SCNPs: $$D_{av.} = 2.18\ \cdot 10^{-10}\frac{m^2}{s};\ (averaged\ four\ values)$$

$$R_h = 1.85 \cdot 10^{-9}\,m = 1.85\ \mathrm{nm}$$

P$_{P/Oxide}$-Eu(dbm)$_3$: $$D_{av.} = 3.59\ \cdot 10^{-1}\ \frac{m^2}{s};\ (averaged\ four\ values)$$

$$R_h = 11.2 \cdot 10^{-9}\,m = 11.2\ \mathrm{nm}$$

DOSY report $P_{P/Oxide}$:

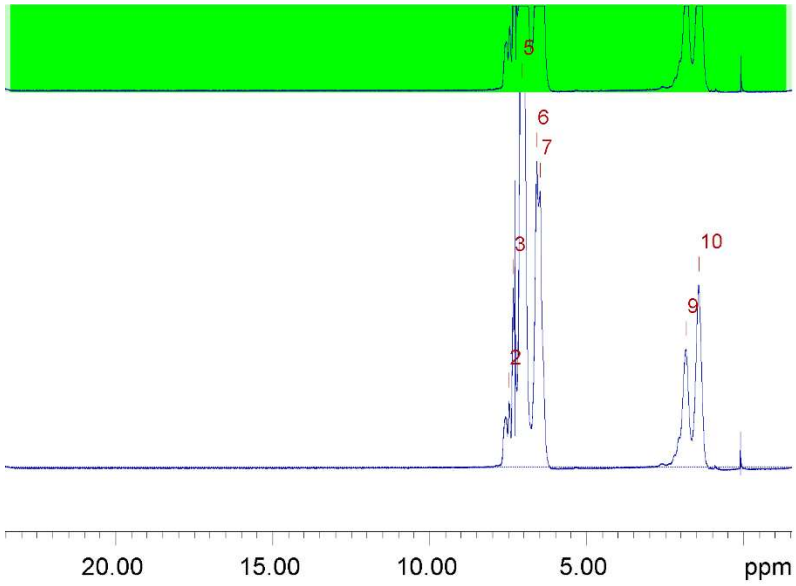

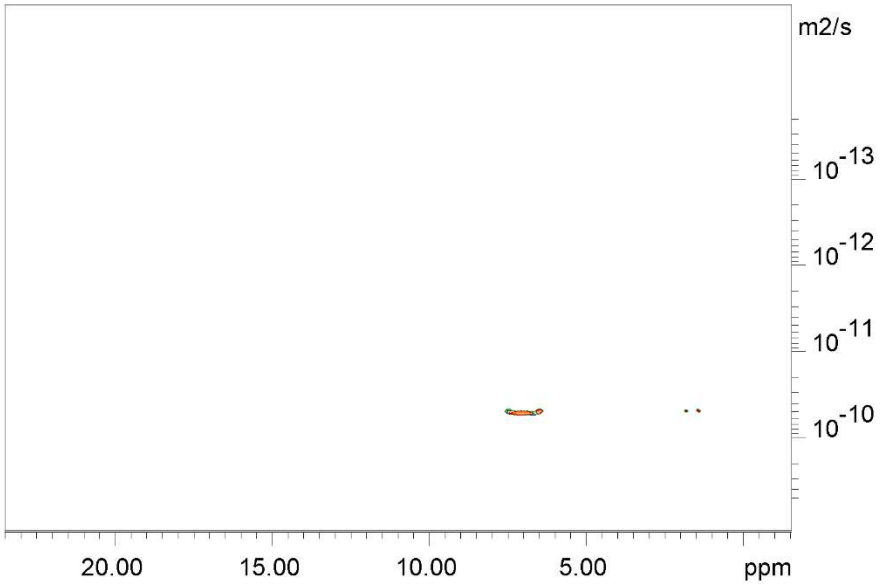

Fitted function:	f (x) = Io * exp (-D * x^2 * gamma^2 * littleDelta^2 (bigDelta-littleDelta/3)* 10^4
used gamma:	26752 rad/(s*Gauss)
used little delta:	0.0040000 s
used big delta:	0.34990 s
used gradient strength:	variable
Random error estimation of data:	RMS per spectrum (or trace/plane)
Systematic error estimation of data:	worst case per peak scenario
Fit parameter Error estimation method:	from fit using arbitray y uncertainties
Confidence level:	95%
Used peaks:	peaks from D:\data\nmr_temp\nmr\patz_BE_083\203\pdata\1\peaklist.xml
Used integrals:	peak intensities
Used Gradient strength:	all values (including replicates) used

Peak name	F2 [ppm]	D [m2/s]	error
2	7.474	5.02e-11	2.996e-13
3	7.339	5.05e-11	1.732e-13
5	7.056	5.04e-11	1.817e-13
6	6.590	5.04e-11	1.685e-13
7	6.488	4.91e-11	1.811e-13
9	1.844	5.00e-11	2.051e-13
10	1.436	5.00e-11	2.023e-13

DOSY report **$Eu_{(dbm)}$(III)/Pt(II)-SCNPs**:

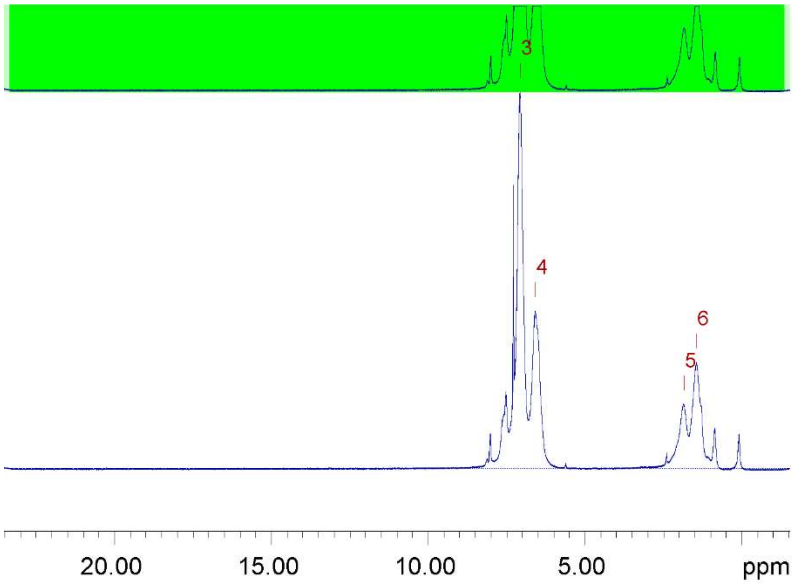

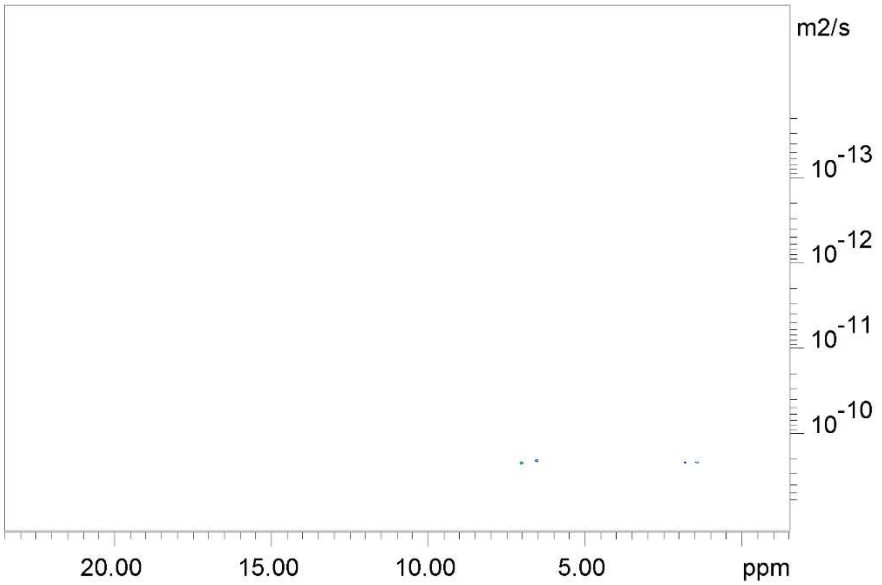

Fitted function:	f (x) = Io * exp (-D * x^2 * gamma^2 * littleDelta^2 (bigDelta-littleDelta/3)* 10^4
used gamma:	26752 rad/(s*Gauss)
used little delta:	0.0020000 s
used big delta:	0.34990 s
used gradient strength:	variable
Random error estimation of data:	RMS per spectrum (or trace/plane)
Systematic error estimation of data:	worst case per peak scenario
Fit parameter Error estimation method:	from fit using arbitray y uncertainties
Confidence level:	95%
Used peaks:	peaks from D:\data\nmr_temp\nmr\patz_BE_084\3\pdata\1\peaklist.xml
Used integrals:	peak intensities
Used Gradient strength:	all values (including replicates) used

Peak name	F2 [ppm]	D [m2/s]	error
3	7.074	2.16e-10	1.196e-12
4	6.589	2.15e-10	1.284e-12
5	1.857	2.17e-10	1.271e-12
6	1.449	2.24e-10	7.936e-13

DOSY report $P_{P/Oxide}$-Eu(dbm)$_3$:

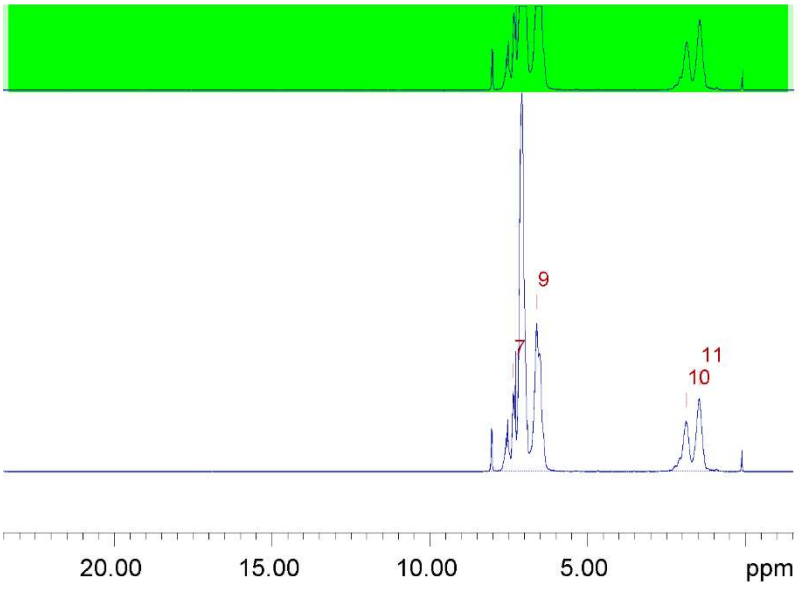

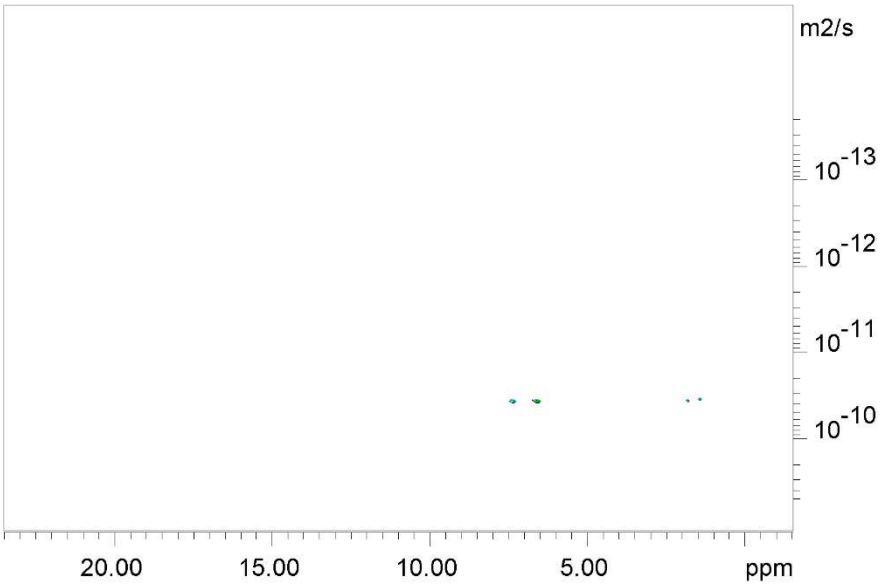

Fitted function:	f (x) = Io * exp (-D * x^2 * gamma^2 * littleDelta^2 (bigDelta-littleDelta/3)* 10^4
used gamma:	26752 rad/(s*Gauss)
used little delta:	0.0042000 s
used big delta:	0.49990 s
used gradient strength:	variable
Random error estimation of data:	RMS per spectrum (or trace/plane)
Systematic error estimation of data:	worst case per peak scenario
Fit parameter Error estimation method:	from fit using arbitray y uncertainties
Confidence level:	95%
Used peaks:	peaks from D:\data\nmr_temp\nmr\patz_BE_087\3\pdata\1\peaklist.xml
Used integrals:	peak intensities
Used Gradient strength:	all values (including replicates) used

Peak name	F2 [ppm]	D [m2/s]	error
7	7.351	3.62e-11	3.281e-13
9	6.610	3.58e-11	2.589e-13
10	1.874	3.58e-11	2.651e-13
11	1.462	3.56e-11	2.707e-13

IR Spectra

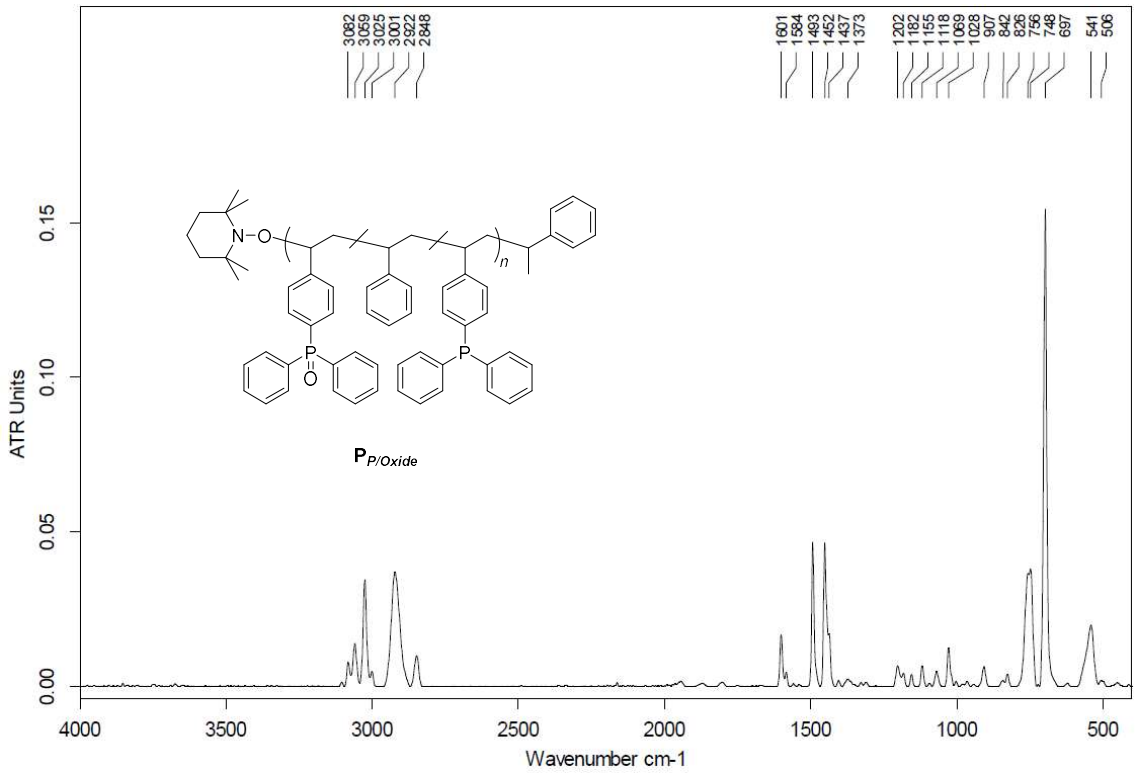

Fig. S22. IR spectrum of $P_{P/Oxide}$.

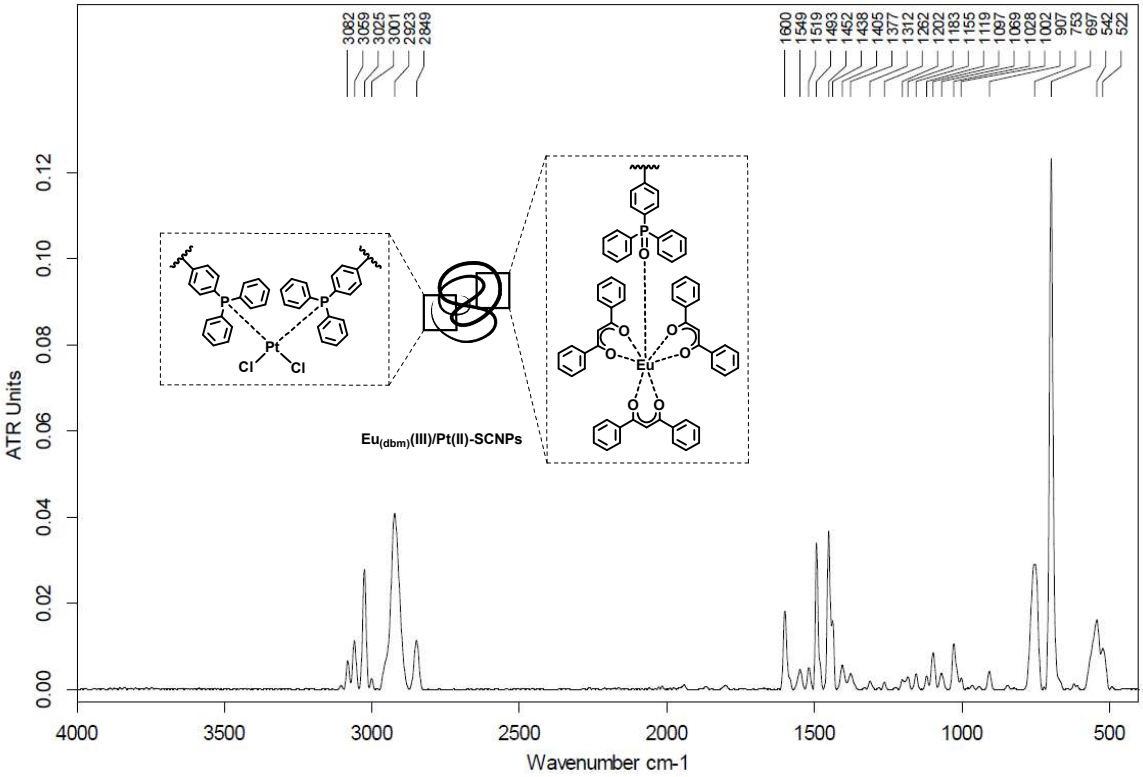

Fig. S23. IR spectrum of $Eu_{(dbm)}(III)/Pt(II)$-SCNPs.

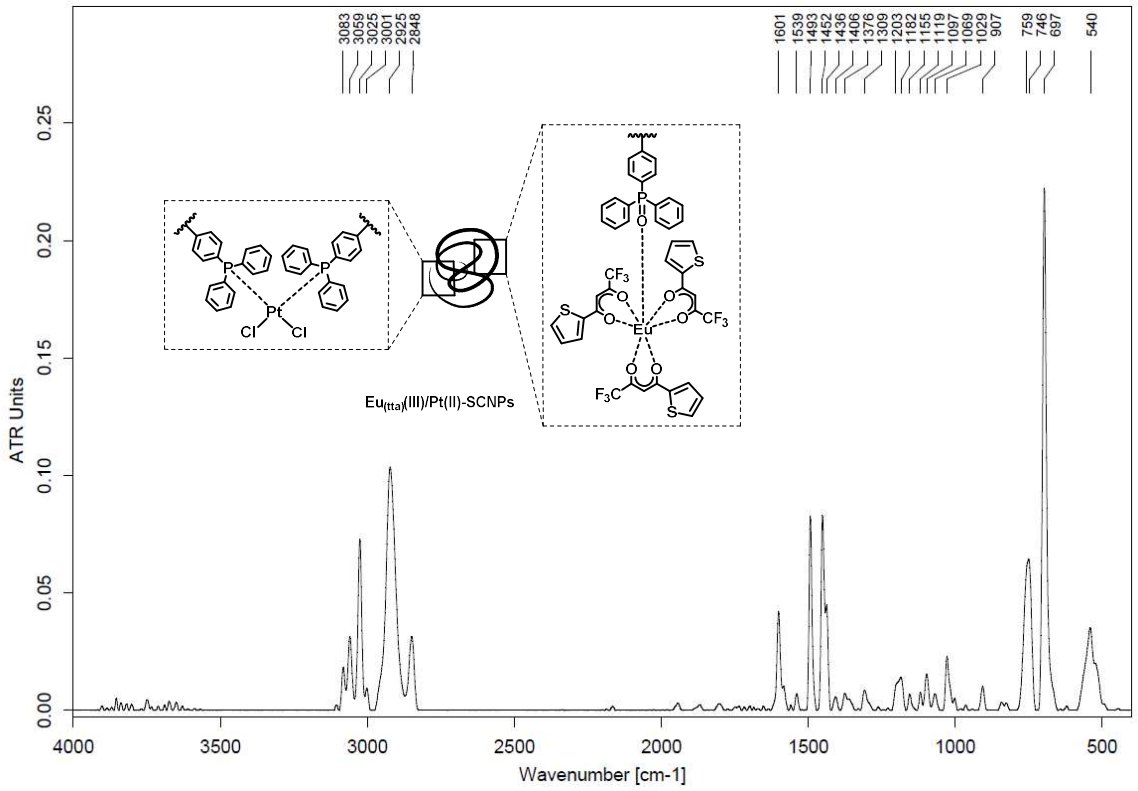

Fig. S24. IR spectrum of **Eu$_{(tta)}$(III)/Pt(II)-SCNPs**.

Photoluminescence Spectra

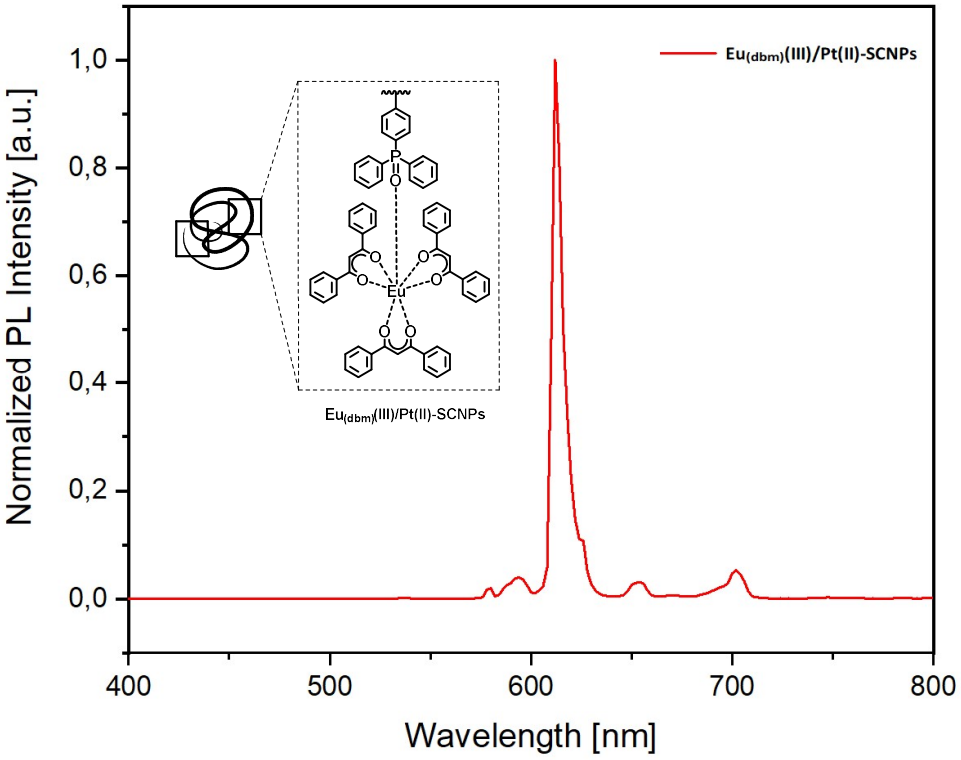

Fig. S25. Photoluminescence emission (PL) spectrum of **$Eu_{(dbm)}$(III)/Pt(II)-SCNPs** in the solid state, after excitation λ = 350 nm (at 298 K). The spectrum exhibits a maximum at λ = 612 nm, resulting from an Eu(III)-centered $^5D_0$-$^7F_2$ transition (4f-4f).[6]

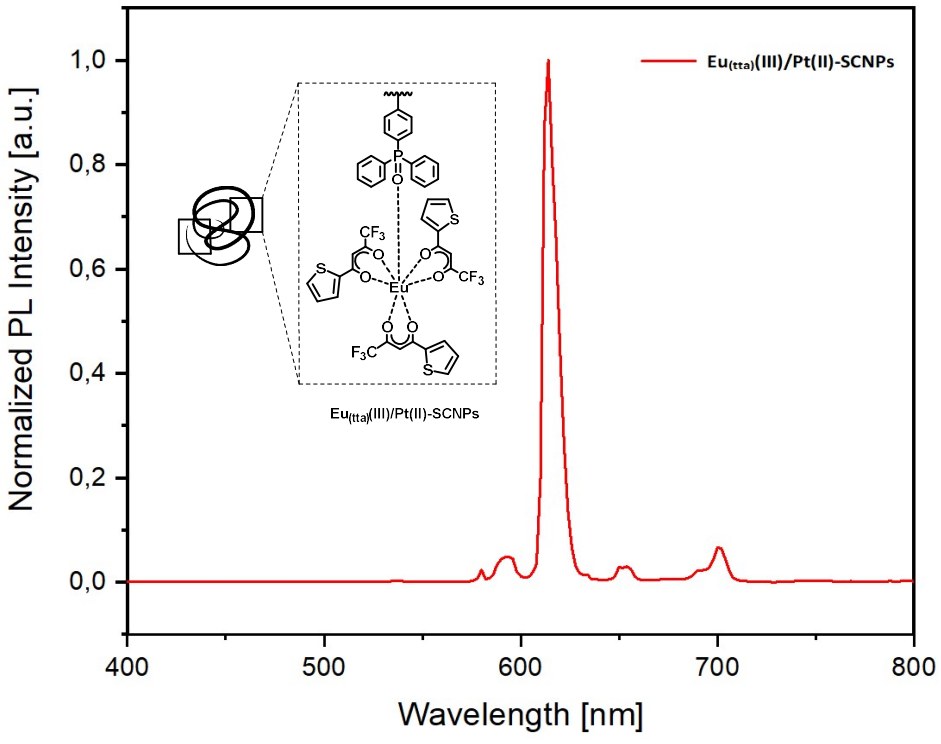

Fig. S26. Photoluminescence emission (PL) spectrum of **$Eu_{(tta)}$(III)/Pt(II)-SCNPs** in the solid state, after excitation λ = 350 nm (at 298 K). The spectrum exhibits a maximum at λ = 614 nm, resulting from an Eu(III)-centered $^5D_0$-$^7F_2$ transition (4f-4f).[6]

Fig. S27. Photograph of **$Eu_{(dbm)}$(III)/Pt(II)-SCNPs** (left) and **$Eu_{(tta)}$(III)/Pt(II)-SCNPs** (right) in the solid state, after excitation at λ = 365 nm.

Catalysis

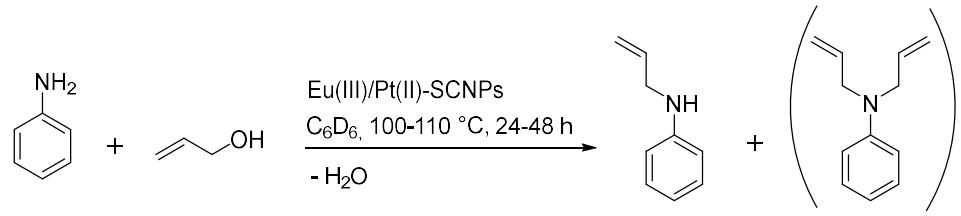

Scheme S6. Reaction of aniline with allyl alcohol catalyzed by **Eu(III)/Pt(II)-SCNPs**.

The reactants aniline (14.9 mg, 0.16 mmol, 2.00 equiv.) and allyl alcohol (4.65 mg, 0.08 mmol, 1.00 equiv.) were added to a Young NMR tube, containing **Eu(III)/Pt(II)-SCNPs** (20.0 mg, 0.0032 mmol, 0.04 equiv. with regards to the Pt(II) species), ferrocene (1.49 mg, 0.008 mmol, 0.10 equiv.) and molecular sieves (3 Å). The reaction mixture was dissolved in ca. 0.4 mL C_6D_6 and purged with argon for 5 minutes. Subsequently, the NMR tube was placed in a drying oven at 100-110 °C for 24 h (respectively 48 h). – Catalysis was performed for both **$Eu_{(tta)}$(III)/Pt(II)-SCNPs** and **$Eu_{(dbm)}$(III)/Pt(II)-SCNPs**, applying 4 mol% of catalytically active Pt(II) species (equals 2 mol% of Eu(III) species) in each case. Hereby, the nanoparticles featuring the tta modified Eu(III) complexes exhibit a visibly more intense luminescence. A similar catalytic study has previously been investigated for sole Pt(II)-SCNPs, which proved a high catalytic activity even at catalyst concentrations of 0.24 mol%.[4] To allow a straightforward catalyst detection via illumination with UV-light, in the current approach a higher catalyst loading was applied, mainly with regards to the amount of Eu(III) species (which is partially quenched by the starting materials aniline and allyl alcohol, as well as the nascent H_2O during the reaction).

The conversion and selectivity were determined by ^{1}H NMR spectroscopy with ferrocene as an internal standard. The ratio between ferrocene, the reactant allyl alcohol and the product(s) was calculated by integral comparison of the corresponding proton resonances (-C*H*$_2$ respectively =C*H*) in the ^{1}H NMR spectrum (see Fig. S28-S32). The ^{1}H NMR data of the product(s) match with the literature.[7-8] Since an excess (two equivalents) of aniline was applied, residual peaks appear in the spectra at t = 24 h and t = 48 h, respectively (Fig. S30 and S32). Conversion numbers, applying the different SCNP systems, may differ due to statistically distributed platinum centers and weighing errors.

The **Eu(III)/Pt(II)-SCNPs** can be separated after the catalysis by precipitation in methanol and/or subsequent column chromatography (*e.g.* neutral aluminium oxide, acetone), where they remain on top of the column and are readily detected by UV-light illumination (see Fig. 5 main paper; illustrating the example of **$Eu_{(tta)}$(III)/Pt(II)-SCNPs** as catalyst). UV illumination of the filtrate after column chromatography showed no luminescence, thus indicating a complete catalyst separation. Alternatively, precipitation and separation of the SCNPs can be achieved via addition of cold methanol to the reaction mixture or applying dialysis in methanol.[4] However, applying protic solvents as methanol leads to an increased quenching of the Eu(III) luminescence.

With increasing reaction time, the intensity of the luminescence decreases during catalysis, most likely due to the formation of H_2O which leads to a partial quenching of the Eu(III) species (Fig. S33). Additionally, as observed for the **$Eu_{(tta)}$(III)/Pt(II)-SCNPs** via ^{19}F NMR studies, the dikentonate ligands of the Eu(III) complex are partially removed with increasing reaction temperature and time. However, a temperature below 90 °C merely results in low yields in case of the reaction between aniline and allyl alcohol. Additionally, in the eluant of the chromatography a weak resonance in the ^{19}F NMR spectrum is detected, attributed to unbound tta ligands, confirming partial decomposition during catalysis.

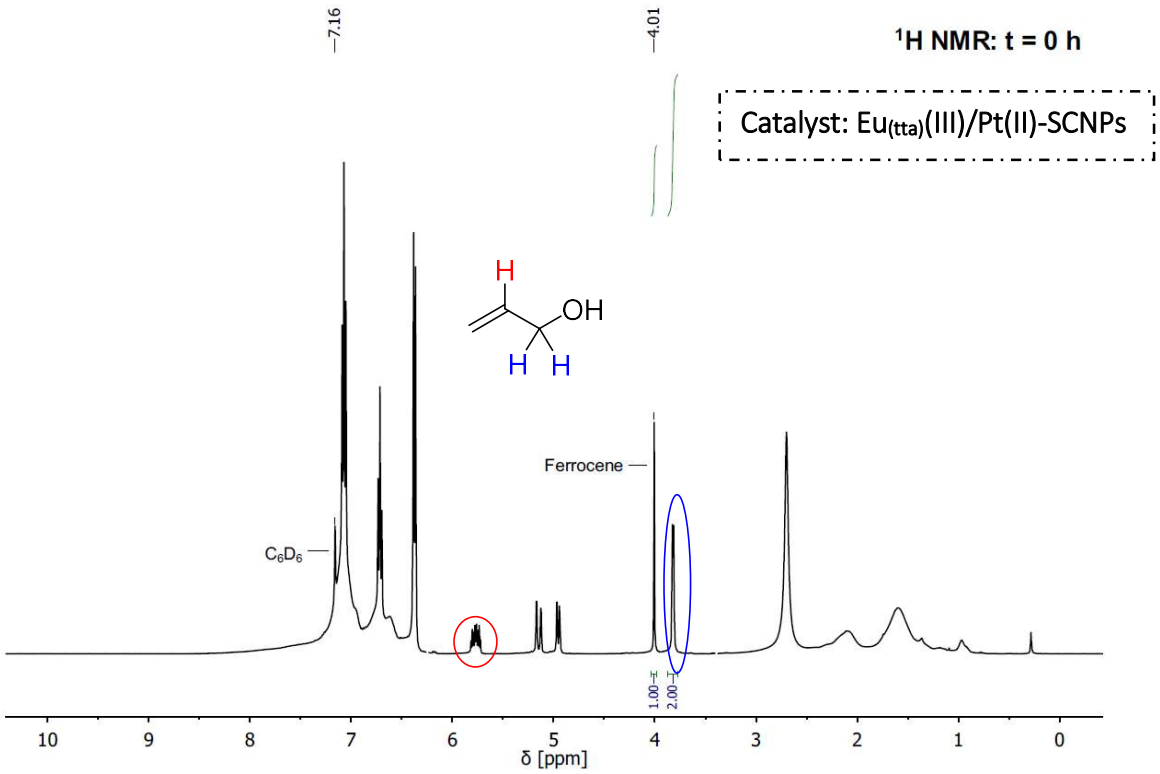

Fig. S28. ^{1}H NMR spectrum at t = 0 h, which defines the start of the reaction. NMR measurement was performed in C_6D_6 and ferrocene was used as an internal standard. In this case **$Eu_{(tta)}$(III)/Pt(II)-SCNPs** were applied as catalyst.

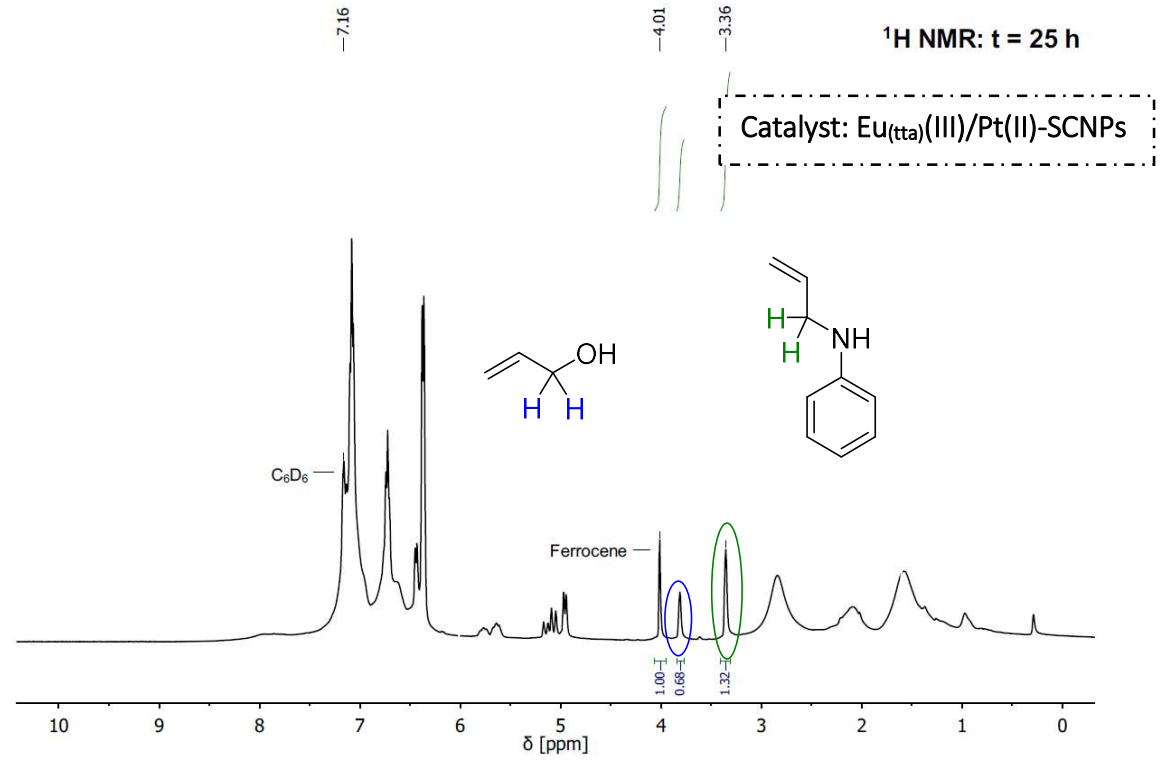

Fig. S29. ^{1}H NMR spectrum at t = 25 h. Analysis resulted in an allyl alcohol conversion of about 67 %. Catalysis and NMR measurement were performed in C_6D_6 and ferrocene was used as an internal standard. In this case **$Eu_{(tta)}$(III)/Pt(II)-SCNPs** were applied as catalyst.

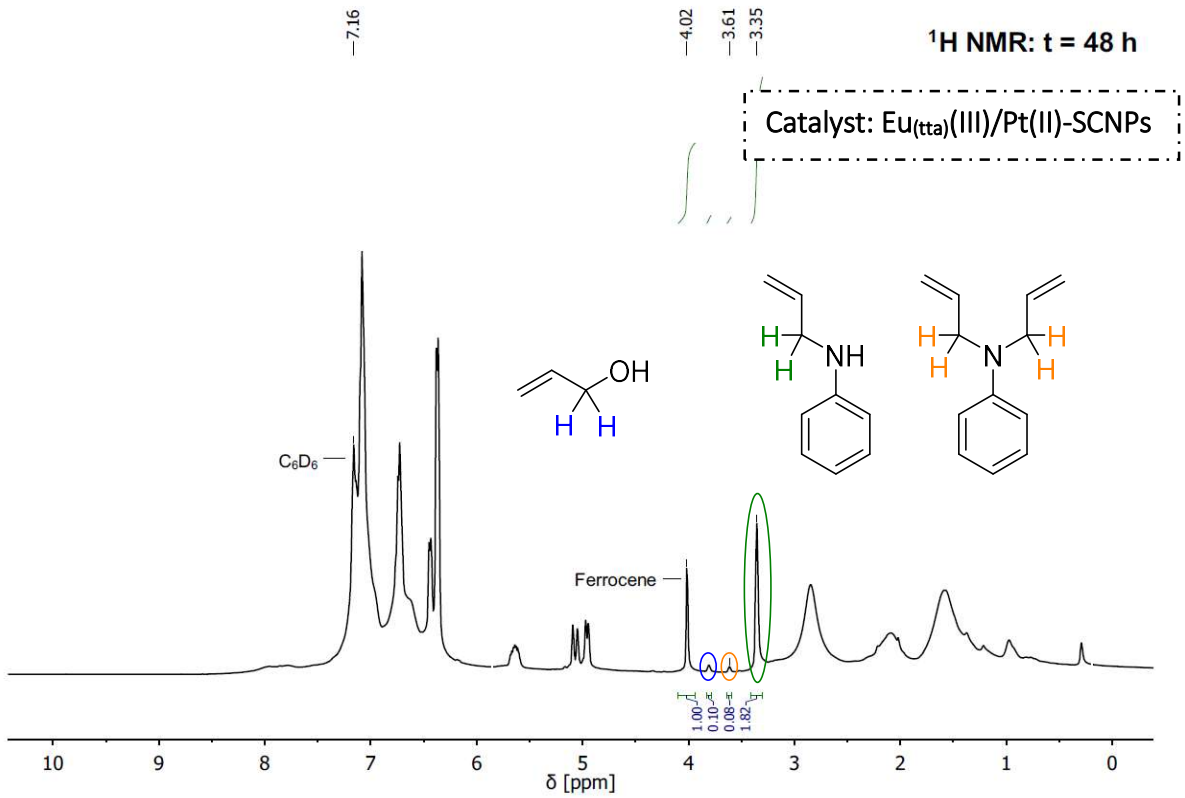

Fig. S30. ^{1}H NMR spectrum at t = 48 h. Analysis resulted in an allyl alcohol conversion of about 91 %. Catalysis and NMR measurement were performed in C_6D_6 and ferrocene was used as an internal standard. In this case **$Eu_{(tta)}$(III)/Pt(II)-SCNPs** were applied as catalyst.

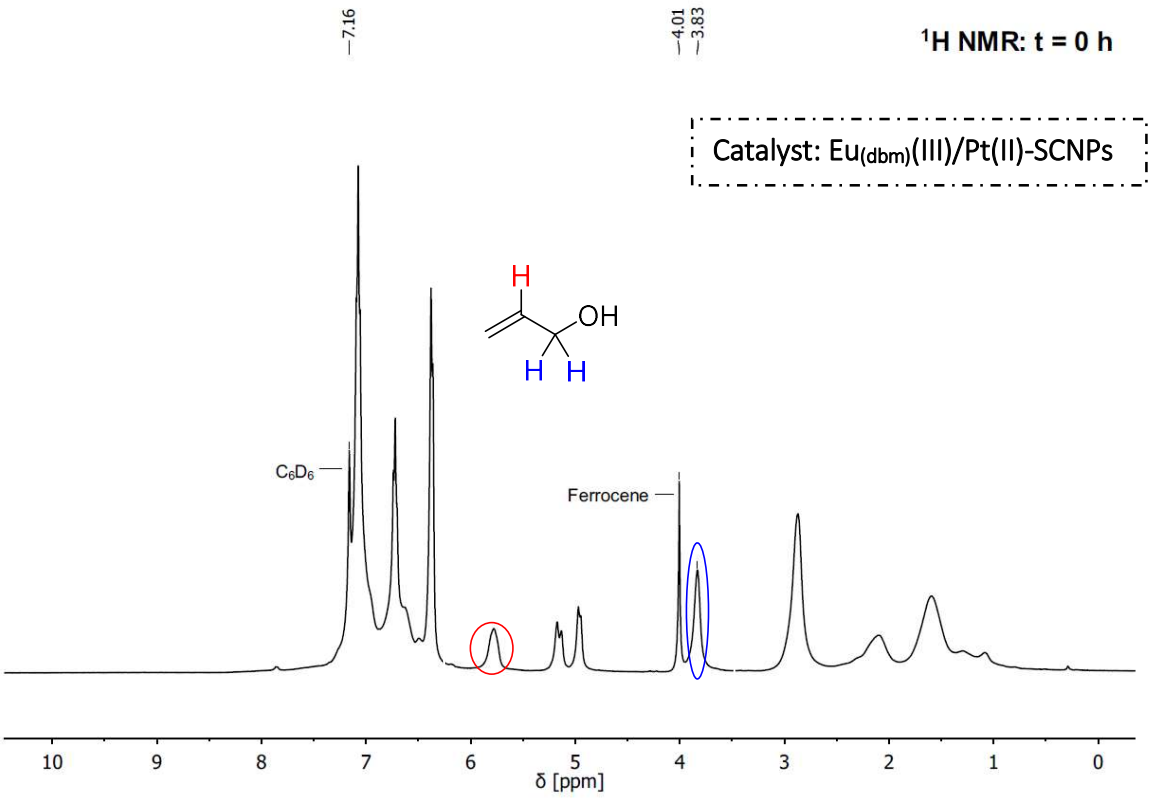

Fig. S31. ^{1}H NMR spectrum at t = 0 h, which defines the start of the reaction. NMR measurement was performed in C_6D_6 and ferrocene was used as an internal standard. In this case **$Eu_{(dbm)}$(III)/Pt(II)-SCNPs** were applied as catalyst.

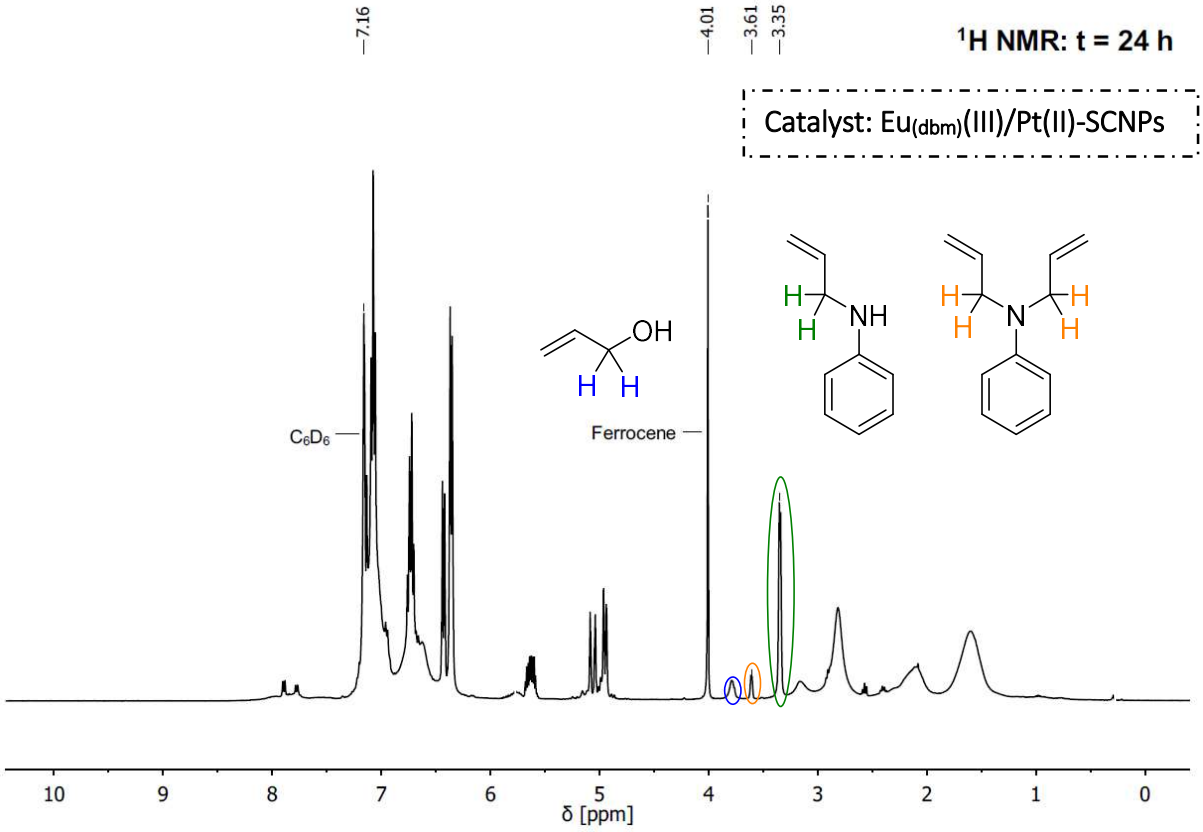

Fig. S32. ^{1}H NMR spectrum at t = 24 h. Analysis resulted in an allyl alcohol conversion of about 85 %. Catalysis and NMR measurement were performed in C_6D_6 and ferrocene was used as an internal standard. In this case **$Eu_{(dbm)}$(III)/Pt(II)-SCNPs** were applied as catalyst.

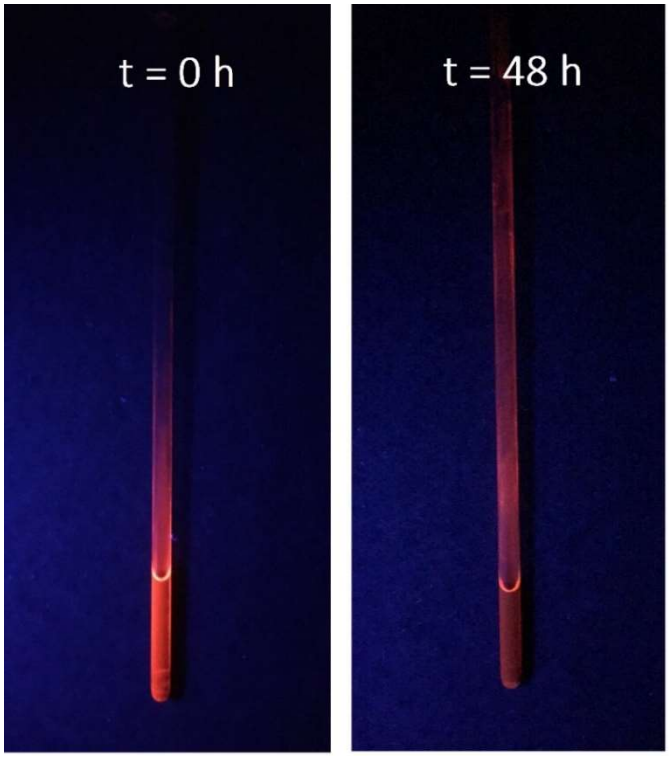

Fig. S33. Photographs of the catalysis reaction mixture (Young NMR tube; in C_6D_6) containing the fluorescent **$Eu_{(tta)}$(III)/Pt(II)-SCNPs** at the times t = 0 h (left) and t = 48 h (right), after excitation at λ = 365 nm. The photoluminescence is slightly reduced after 48 h, most likely due to the formation of H_2O and partial quenching of the Eu(III) species.

References

[1] A. Kusumaatmaja, T. Ando, K. Terada, S. Hirohara, T. Nakashima, T. Kawai, T. Terashima, M. Tanihara, *J. Polym. Sci., Part A: Polym. Chem.* **2013**, *51*, 2527.

[2] N. B. D. Lima, A. I. S. Silva, P. C. Gerson Jr., S. M. C. Gonçalves, A. M. Simas, *PLoS One* **2016**, *10*, e0143998.

[3] J. G. White, *Inorg. Chim. Acta* **1976**, *16*, 159.

[4] N. D. Knöfel, H. Rothfuss, J. Willenbacher, C. Barner-Kowollik, P. W. Roesky, *Angew. Chem. Int. Ed.* **2017**, *56*, 4950.

[5] D. R. Lide, *CRC Handbook of Chemistry and Physics, 85th Ed.*, Taylor & Francis, **2004**.

[6] N. B. D. Lima, S. M. C. Gonçalves, S. A. Júnior, A. M. Simas, *Sci. Rep.* **2013**, *3*, 2395.

[7] S. Sawadjoon, A. Orthaber, P. J. R. Sjöberg, L. Eriksson, J. S. M. Samec, *Organometallics* **2014**, *33*, 249.

[8] B. Schmidt, S. Krehl, E. Jablowski, *Org. Biomol. Chem.* **2012**, *10*, 5119.